

1
2
3
4
5
6
7
8
9
10
11
12
13
14
15
16
17
18
19

Article type: **Research Advances**

**Axon-dependent expression of YAP/TAZ mediates Schwann cell remyelination
but not proliferation after nerve injury**

Matthew Grove^{1,2}, Hyunkyung Lee^{1,2}, Huaqing Zhao³, and Young-Jin Son^{1,2*}

¹Shriners Hospitals Pediatric Research Center and Center for Neural Repair and Rehabilitation,
²Department of Anatomy and Cell Biology, ³Department of Clinical Sciences, Lewis Katz
School of Medicine, Temple University, Philadelphia, PA 19140

* Corresponding author: Young-Jin Son, PhD
Tel: (215) 926-9354
Email: yson@temple.edu

20 **ABSTRACT**

21

22 Previously we showed that YAP/TAZ promote not only proliferation but also differentiation of
23 immature Schwann cells (SCs), thereby forming and maintaining the myelin sheath around
24 peripheral axons (Grove et al., 2017). Here we show that YAP/TAZ are required for mature SCs
25 to restore peripheral myelination, but not to proliferate, after nerve injury. We find that
26 YAP/TAZ dramatically disappear from SCs of adult mice concurrent with axon degeneration
27 after nerve injury. They reappear in SCs only if axons regenerate. YAP/TAZ ablation does not
28 impair SC proliferation or transdifferentiation into growth promoting repair SCs. SCs lacking
29 YAP/TAZ, however, fail to upregulate myelin-associated genes and completely fail to
30 remyelinate regenerated axons. We also show that both YAP and TAZ are redundantly required
31 for optimal remyelination. These findings suggest that axons regulate transcriptional activity of
32 YAP/TAZ in adult SCs and that YAP/TAZ are essential for functional regeneration of peripheral
33 nerve.

34

35 INTRODUCTION

36 YAP (Yes-associated protein) and TAZ (Transcriptional coactivator with PDZ-binding motif),
37 are paralogous transcription coactivators, chiefly known as potent stimulators of cellular
38 proliferation in diverse developing (von Gise et al., 2012; Zhang et al., 2012; Xin et al., 2013;
39 Cotton et al., 2017) and neoplastic (Yu et al., 2015; Zanconato et al., 2016; Moon et al., 2018)
40 tissues. Consistent with this role, we and others have recently shown that YAP/TAZ promote
41 vigorous proliferation of immature Schwann cells (SC) in developing peripheral nerves (Poitelon
42 et al., 2016; Deng et al., 2017; Grove et al., 2017), and that overexpression of YAP/TAZ
43 promotes abnormally excessive proliferation of mature SCs in adult peripheral nerves (Mindos et
44 al., 2017; Wu et al., 2018). Unexpectedly, several groups demonstrated that YAP or YAP/TAZ
45 promote differentiation of developing SCs by upregulating myelin-associated genes, thereby
46 mediating developmental myelination (Fernando et al., 2016; Lopez-Anido et al., 2016; Poitelon
47 et al., 2016; Deng et al., 2017; Grove et al., 2017). Our group additionally showed that
48 YAP/TAZ are selectively expressed in differentiated myelin-forming SCs, and that they are
49 required for maintenance of the myelin sheath in adult nerves (Grove et al., 2017). In many
50 systems, YAP/TAZ shift to the cytoplasm concomitant with differentiation of developing cells,
51 and the nuclear exclusion of YAP/TAZ is believed to be required for homeostatic maintenance of
52 mature cells or tissues (Varelas, 2014; Wang et al., 2018). We were therefore intrigued to find
53 that YAP/TAZ are nuclear and transcriptionally active in mature SCs maintaining peripheral
54 myelination.

55

56 Building on these findings in developing and intact adult nerves, we now report on the role of
57 YAP/TAZ in the regenerating nerve, in which SCs both proliferate and differentiate, as in
58 developing peripheral nerve. Following traumatic nerve injury, SCs in axotomized nerve rapidly
59 dedifferentiate and proliferate as they convert to regeneration promoting “repair” SCs (Jessen
60 and Mirsky, 2016; Tricaud and Park, 2017). When repair SCs regain axon contacts, they re-
61 differentiate to myelin-forming SCs, thereby restoring motor and sensory functions (Fex
62 Svennigsen and Dahlin, 2013; Stassart et al., 2013). Strikingly, we found that YAP/TAZ
63 disappear from denervated SCs but reappear in SCs as axons regenerate. Consistent with these
64 observations, we found that YAP/TAZ are dispensable for SC proliferation after injury but
65 required for remyelination of regenerated axons. These findings extend the role of YAP/TAZ to

66 functional regeneration of injured nerves and suggest that SCs are dependent on axons for their
67 transcriptional activity of YAP/TAZ.

68

69 **RESULTS**

70

71 **YAP/TAZ expression in Schwann cells is axon-dependent**

72 Transcriptional regulation of SC proliferation and differentiation by YAP/TAZ depends on their
73 nuclear localization. Nuclear YAP/TAZ in SCs of adult mice promote myelin gene expression,
74 essentially maintaining peripheral nerve myelination (Grove et al., 2017). As the first step to
75 determine the roles of YAP/TAZ in nerve repair, we examined spatiotemporal expression
76 patterns of YAP/TAZ in adult mice after sciatic nerve crush injury (Figure 1). The nerve crush
77 model evokes active axon degeneration in the distal nerve stump, while permitting new axons
78 from the proximal nerve stump to regenerate through the crushed site within 1-2 days post injury
79 (dpi) (Kang and Lichtman, 2013; Jang et al., 2016; Frenzo et al., 2019). New axons then keep
80 regenerating within the basal lamina tubes filled with SCs and their processes, at the speed of 1-4
81 mm/day, although the debris of degenerating axons and myelin is not yet completely removed.
82 We killed these mice 1, 3, 6, 9, 12, and 24 dpi and immunostained proximal and distal nerve
83 stumps of ~5 mm in length with an antibody specific for both YAP and TAZ (Figure 1A; at 12
84 dpi). At 1 dpi when distal axons remained largely intact, nuclear expression of YAP/TAZ in
85 associated SCs was unchanged (Figure 1B; 1D-dstl). Strikingly, at 3 dpi when axon degeneration
86 was robust and SCs lost axon contacts, YAP/TAZ were almost undetectable in SC nuclei (Figure
87 1B; 3D-dstl). Thus, SCs lose nuclear expression of YAP/TAZ as associated axons degenerate.

88

89 YAP/TAZ reappeared in the nuclei of SCs at 6 dpi, and these SCs were associated with
90 regenerating axons (Figure 1B; 6D-dstl). By 12 dpi, as axon regeneration and maturation
91 progressed further, more SCs exhibited strong nuclear expression of YAP/TAZ, comparable to
92 that of SCs in the proximal nerve stumps (Figure 1B; 12D-dstl, see also Figure 1A). These
93 observations suggest that SCs upregulate nuclear YAP/TAZ, when they regain axon contacts as
94 axons regenerate.

95

96 Notably, we frequently observed thin regenerating axons associated with SCs at 3dpi, but
97 YAP/TAZ were undetectable in these SCs (Figure 1B; zoomed area of 3D-dstl). In contrast, SCs
98 exhibiting strong YAP/TAZ at 6- and 12 dpi were associated with thick axons, which appeared
99 large enough to be myelinated (i.e., $1 > \mu\text{m}$; Figure 1B; 6D-dstl, zoomed area of 12D-dstl). These
100 observations suggest that YAP/TAZ are selectively upregulated in SCs associated with
101 regenerating axons that have become large enough to be myelinated. Consistent with this notion,
102 YAP/TAZ are expressed in myelinating, but not in non-myelinating, SCs (Grove et al., 2017).

103

104 Western blotting also revealed marked reduction of YAP and TAZ levels at 3 dpi, followed by
105 rapid upregulation of TAZ levels (Figure 1C, Figure 1-source data 2). Notably, YAP levels
106 remained low in nerve lysates at 12 dpi (Figure 1C). As cells other than SCs can affect overall
107 YAP levels (Gaudet et al., 2011; Stierli et al., 2018), we next examined expression of YAP in
108 SCs of crushed nerves by immunohistochemistry (IHC). We first verified that an antibody
109 specifically recognized YAP, but not TAZ (Figure 1-figure supplement 1A). YAP is upregulated
110 in many SC nuclei at 6 dpi and continues to be observed at 24 dpi (Figure 1-figure supplement
111 1B), demonstrating that YAP is also upregulated in SCs concomitant with axon regeneration.

112

113 The dramatic down- and upregulation of YAP/TAZ concurrent with axon degeneration and
114 regeneration, respectively, suggest that SCs are dependent on axons for YAP/TAZ nuclear
115 expression. To test further whether axons regulate YAP/TAZ expression in mature SCs, we next
116 investigated if denervated SCs are capable of upregulating YAP/TAZ in the absence of
117 regenerating axons. We used a nerve transection injury model in which we completely cut one
118 sciatic nerve and tied both ends of the transected nerve to prevent axon regeneration from
119 proximal to distal nerve stumps. We examined these mice at 1, 3, 6, 9, 12, and 24 dpi. We first
120 confirmed absence of regenerating axons in distal nerve stumps of these mice and found that
121 YAP/TAZ become undetectable in SCs at 3 dpi (Figure 2B; 3D-dstl), concurrent with robust
122 axon degeneration as observed after nerve crush injury. Notably, nuclear YAP/TAZ continued to
123 be undetectable in SCs after 3 dpi (Figure 2B; e.g., 12D-dstl, see also Figure 2A), demonstrating
124 that axons are required for YAP/TAZ upregulation in denervated SCs.

125

126 We also used an antibody specific for transcriptionally inactive, phosphorylated YAP (p-YAP),
127 which is located preferentially in cytoplasm and exhibits perinuclear and membrane
128 accumulation (Grove et al., 2017). We found that p-YAP became undetectable in SCs of
129 transected/tied nerves by 12 dpi (Figure 2C). In contrast, p-YAP expression recovered in SCs of
130 crushed nerves at 12 dpi (Figure 2D). These findings suggest that SCs are dependent on axons
131 for both nuclear and cytoplasmic expression of YAP/TAZ.

132

133 **YAP/TAZ are dispensable for Schwann cell proliferation after nerve injury**

134 SCs rapidly dedifferentiate and convert to repair SCs after nerve injury. During this
135 transdifferentiation process, SCs begin to proliferate ~3 dpi (Clemence et al., 1989; Jessen and
136 Mirsky, 2016; Tricaud and Park, 2017). Our observation that YAP/TAZ disappear in SCs by 3
137 days after axotomy raises the interesting possibility that YAP/TAZ are not involved in injury-
138 elicited SC proliferation. Alternatively, levels of YAP/TAZ that are too low to be detected by
139 IHC may be sufficient to promote transcription of the genes activating SC proliferation. To test
140 these possibilities, we used an inducible knockout mouse (*Plp1-creERT2; Yap^{fl/fl}; Taz^{fl/fl}*,
141 hereafter Yap/Taz iDKO) to inactivate YAP/TAZ selectively in SCs after nerve injury. We
142 induced recombination at 6 weeks of age, completely transected and tied the sciatic nerve in one
143 leg, killed the mice 5 days later when SCs actively proliferate, and compared SC proliferation in
144 intact and transected nerves of WT and iDKO mice (Figure 3A, n=3 mice per genotype). We first
145 confirmed efficient ablation of YAP/TAZ in SCs by analyzing contralateral, intact nerves of
146 iDKO mice (Figure 3B, 3F). We excluded mice with poor deletion (i.e., exhibiting YAP/TAZ in
147 >20% SCs) from further analysis. Notably, pulse labeling with EdU indicated that the transected
148 nerves of WT and iDKO contained similar numbers of dividing SCs in S phase (Figure 3C, 3G).
149 Numbers of Ki67+ proliferating SCs (Figure 3D, 3H) and of total SCs (Figure 3E, 3I) were also
150 similar in the transected nerves of WT and iDKO.

151

152 If adult SCs lacking YAP/TAZ in iDKO die or proliferate independently of axotomy, our
153 analysis of injury-elicited SC proliferation might be confounded. To exclude this possibility, we
154 examined contralateral, intact nerves of WT and iDKO mice at 12 dpi for SC proliferation and
155 death (Figure 3-figure supplement 1A). Contralateral iDKO nerves contained neither EdU+ SCs
156 (Figure 3-figure supplement 1B) nor apoptotic SCs, as assessed by TUNEL assays (Figure 3-

157 figure supplement 1C). We also found that SC numbers did not differ significantly from those in
158 intact nerves of WT mice (Figure 3-figure supplement 1D, 1E). Collectively, these results
159 strongly indicate that YAP/TAZ do not regulate SC proliferation after nerve injury.

160

161 **SCs lacking YAP/TAZ convert to repair SCs and support axon regeneration**

162 Next, we investigated if transdifferentiation to repair SCs proceeds normally in iDKO nerves
163 after injury. We first examined expression of c-Jun, phosphorylated c-Jun (pc-Jun), p75 and Oct-
164 6, which are associated with formation of repair SCs during nerve regeneration (Scherer et al.,
165 1994; Parkinson et al., 2008; Arthur-Farraj et al., 2012; Fontana et al., 2012). Repair SC
166 formation principally depends on the upregulation of c-Jun, which promotes expression of
167 regeneration-associated genes (RAG), such as p75 neurotrophin receptor (NTR) (Parkinson et al.,
168 2008; Arthur-Farraj et al., 2012; Fontana et al., 2012). Immunohistochemical analysis of
169 transected sciatic nerves at 5 dpi showed that cJun, pc-Jun, p75 NTR and Oct-6 were all
170 upregulated in denervated SCs of iDKO mice after nerve injury, as in WT mice (Figure 4, Figure
171 4-figure supplement 1 and Figure 4-source data 3). Notably, injured nerves of WT and iDKO
172 mice contained similar numbers of SCs expressing c-Jun (Figure 4A, 4E) and active pc-Jun
173 (Figure 4B, 4F). There was minimal expression of c-Jun in contralateral, intact nerves of iDKO
174 at 5 dpi (Figure 4-figure supplement 1). p75 NTR expression was also strongly upregulated in
175 iDKO SCs, as in WT SCs (Figure 4C, 4G), and Oct-6 expression in WT and iDKO SCs did not
176 differ (Figure 4D, 4H). Western blotting analysis confirmed upregulation of these proteins in
177 injured nerves and validated the specificity of the antibodies used in the immunohistochemical
178 analysis (Figure 4-figure supplement 1 and Figure 4-source data 3).

179

180 SCs are essential for successful nerve regeneration (Scheib and Hoke, 2013; Jessen and Mirsky,
181 2016). As the definitive test of whether iDKO SCs convert normally to repair SCs, we next
182 examined if the absence of YAP/TAZ in SCs impairs nerve regeneration. Because *Yap/Taz*
183 iDKO mice die ~14 days after tamoxifen treatment (Grove et al., 2017), we crushed sciatic
184 nerves and analyzed them on 12-13 dpi. To minimize variability, we crushed nerves at the same
185 site close to the sciatic notch and analyzed nerve segments immunohistochemically or
186 ultrastructurally at the same distance distal to the injury (Figure 5A). An anti- β 3 tubulin antibody,
187 which identifies all axons, intensely labeled many axons that had regenerated through the ~10

188 mm long distal nerve stumps of iDKO mice (Figure 5B, 5D). These axons were as thick and
189 numerous in iDKO as in WT nerves (Figure 5B, 5F, see also Figure 7-figure supplement 1).
190 Similar numbers of axons were also present in contralateral intact nerves of WT and iDKO
191 (Figure 7-figure supplement 1), indicating that there was no axon degeneration in intact nerves of
192 iDKO at 12-13 dpi.

193

194 To confirm these findings, we examined transverse nerve segments 5 mm distal to the injury by
195 TEM (Transmission Electron Microscopy). In this ultrastructural analysis, we took advantage of
196 the fact that regenerating axons extend through the basal lamina (BL) tubes that surround SCs
197 and their processes (Scheib and Hoke, 2013; Jessen and Mirsky, 2016). We found that the
198 percentage of BL tubes containing axons (single or multiple) was similar in WT and iDKO
199 nerves (Figure 5E, 5G). Furthermore, the percentage of BL tubes containing axons large enough
200 to be myelinated (i.e., $>1\mu\text{m}$) did not differ (Figure 5H). However, the large axons in iDKO
201 nerves were more frequently accompanied by one or multiple, often thin, axons, which
202 presumably represent transient collateral sprouts (Figure 5E-d, 5I).

203

204 Next, we examined iDKO nerves at an earlier time point after injury to investigate if axon
205 regeneration might be delayed in the absence of YAP/TAZ in SCs. We analyzed longitudinal
206 sections of crushed sciatic nerves from WT and iDKO mice at 3 dpi (Figure 6; n=3 mice per
207 genotype). Because abundant debris of degenerating axons often confounded
208 immunohistochemical identification of regenerating axons at this early time point, we selectively
209 labeled regenerating axons with an antibody for superior cervical ganglion 10 (SCG10), which is
210 rapidly and preferentially upregulated in sensory axons after injury (Shin et al., 2014; Mogha et
211 al., 2016). Numerous axons reached ~4mm distal to the crush site in iDKO, as in WT mice
212 (Figure 6A, B). There was no significant difference in axon density measured 2 mm distal to the
213 crush (Figure 6C-E), nor in the length of the longest axons (Figure 6F). Taken together, these
214 results show that SCs lacking YAP/TAZ convert normally to repair SCs and support axon
215 regeneration after injury.

216

217 **YAP/TAZ are required for Schwann cells to remyelinate axons**

218 We have previously reported that developing SCs lacking YAP/TAZ arrest as promyelinating
219 SCs, and are therefore unable to initiate myelin formation (Grove et al., 2017). To determine if
220 adult SCs lacking YAP/TAZ can myelinate regenerating axons, we next analyzed the extent of
221 myelination in the same iDKO nerves analyzed for axon regeneration on 12-13 dpi (Figure 7A
222 shows the same nerves as Figure 5B). As expected, there was strong expression of myelin basic
223 protein (MBP), a major structural component of the myelin sheath, in the crushed nerves of WT
224 mice (Figure 7A, 7B). MBP immunoreactivity was also abundant in the contralateral, intact
225 nerves of iDKO mice (Figure 7A; bottom panel), in which our previous ultrastructural analysis
226 found segmental demyelination (Grove et al., 2017). In contrast, iDKO crushed nerves revealed
227 remarkably little, if any, MBP immunoreactivity (Figure 7A, 7C, see also Figure 7-figure
228 supplement 1 for higher magnification images). Consistent with this immunohistochemical
229 analysis, semithin (Figure 7D) and ultrathin sections processed for EM (Figure 5E, 7E) contained
230 many myelinated axons in WT but almost none in iDKO crushed nerves (Figure 7F, 7G).
231 Moreover, iDKO SCs frequently surrounded and established a 1:1 relationship with large axons,
232 but none of these axons exhibited a myelin sheath (Figure 5E, 7E). These findings suggest that
233 adult SCs lacking YAP/TAZ fail to remyelinate axons because they arrest at the promyelinating
234 stage after injury.

235

236 **YAP and TAZ are functionally redundant and required for optimal remyelination**

237 Mindos et al. recently reported that expression of YAP, assessed by Western blotting, selectively
238 increases after nerve injury in mutant nerves lacking Merlin in SCs, but not in WT nerves,
239 whereas TAZ increases in both WT and mutant nerves (Mindos et al., 2017). They also reported
240 that elevated YAP levels prevent axon regeneration and remyelination, and that inactivation of
241 YAP alone is sufficient to restore full functional recovery of the Merlin mutants (Mindos et al.,
242 2017). These observations suggest that the function of TAZ in adult SCs may differ from that of
243 YAP. We next examined axon regeneration and remyelination when SCs express YAP but not
244 TAZ after injury. We reasoned that, if YAP prevents regeneration, regardless of expression
245 levels (see Discussion), and if it differs functionally from TAZ, then we would find axon
246 regeneration and remyelination to be poor.

247

248 Using a TAZ-selective tamoxifen inducible line to inactivate TAZ in SCs (*Plp1-creERT2; Yap^{+/+}*;
249 *Taz^{fl/fl}*, hereafter *Taz* iKO), we crushed sciatic nerves unilaterally and compared the mutants to
250 WT and *Yap/Taz* iDKO mice at 12 dpi. We first confirmed efficient ablation of TAZ and no
251 compensatory elevation of YAP levels in *Taz* iKO (Figure 8A, Figure 8-source data 4). We then
252 used anti- β 3 tubulin antibody to assess axon regeneration up to 15 mm distal to the crushed site
253 (Figure 8-figure supplement 1A, B). We found that regenerating axons were as thick and
254 numerous in *Taz* iKO, as in WT mice (Figure 8-figure supplement 1C, D). Axon density
255 measured at 8~10 mm distal to the crush site showed no significant difference among WT, *Taz*
256 iKO and *Yap/Taz* iDKO nerves (Figure 8B, Figure 8-figure supplement 1E).

257

258 Ultrastructural analysis of nerve segments at 5 mm distal to the injury revealed many BL tubes
259 containing single or multiple axons in *Taz* iKO, as in WT (Figure 8C). These axon-containing
260 BL tubes were as numerous in iKO as in WT and iDKO (Figure 8D). Counts of BL tubes
261 containing axons large enough to be myelinated also did not differ (Figure 8E). Taken together,
262 these results show that axons regenerated as robustly in *Taz* iKO as in WT and iDKO nerves,
263 indicating that SCs expressing only YAP supported axon regeneration.

264

265 We also found that, whereas iDKO nerves contained no myelinated axons (e.g., Figure 7D),
266 myelinated axons were frequent in *Taz* iKO nerves (Figure 8C, 8F), and G-ratios did not differ in
267 *Taz* iKO and WT (Figure 8G), demonstrating that SCs expressing only YAP were capable of
268 myelinating regenerated axons. Notably, however, a significantly smaller percentage of single
269 axons were myelinated in *Taz* iKO than in WT (Figure 8F), indicating that remyelination is less
270 advanced in *Taz* iKO nerves whose SCs express only YAP. Taken together, these results show
271 that YAP, at normal levels (see Discussion), does not prevent axon regeneration or remyelination
272 after injury, and that both YAP and TAZ are required for optimal remyelination.

273

274 **Redifferentiation of Schwann cells lacking YAP/TAZ**

275 Following axon regeneration, denervated SCs that have regained axon contacts downregulate
276 dedifferentiation-associated genes while upregulating genes promoting their differentiation
277 (Stassart et al., 2013; Quintes et al., 2016; Wu et al., 2016). It is possible that YAP/TAZ-
278 deficient iDKO SCs fail to myelinate regenerated axons because their capacity to carry out one

279 or both processes is defective. To test if iDKO SCs correctly downregulate dedifferentiation-
280 associated genes, we compared expression of c-Jun, Ki67 and Oct-6 by WT and iDKO SCs at 5
281 and 12 dpi after crush. The number of c-Jun⁺ SCs was markedly, but similarly, reduced in nerves
282 of both WT and iDKO at 12 dpi (Figure 9A, E), and proliferating SCs were rare (Figure 9B, F).
283 Oct-6 expression was also reduced in both WT and iDKO (Figure 9C, G), although it remained
284 statistically higher in iDKO SCs. These results suggest that iDKO SCs are capable of
285 downregulating dedifferentiation genes and withdraw gradually from dedifferentiation as like
286 WT SCs.

287
288 Lastly, we examined expression of Krox 20 (also known as Egr2), the master transcription factor
289 that drives myelin gene expression (Topilko et al., 1994; Decker et al., 2006). Notably, whereas
290 WT SCs upregulated Krox 20 expression at 12 dpi, concomitant with remyelination, few if any
291 iDKO SCs exhibited Krox 20 immunoreactivity (Figure 9D, H). These results suggest that iDKO
292 SCs fail to myelinate regenerated axons at least in part due to failure to upregulate Krox 20.

293 294 **DISCUSSION**

295 Recent studies of SC-specific gene targeting consistently show that SCs lacking both YAP and
296 TAZ are unable to proliferate properly and fail to myelinate developing peripheral nerves
297 (Poitelon et al., 2016; Deng et al., 2017; Grove et al., 2017). It remains controversial, however,
298 how YAP/TAZ loss results in complete amyelination of developing nerves and whether
299 YAP/TAZ also play a role in myelin maintenance of adult nerves. Indeed, Poitelon et al.,
300 attributed developmental amyelination to the inability of immature SCs lacking YAP/TAZ to
301 wrap around developing axons, a process called radial sorting (Feltri et al., 2016; Poitelon et al.,
302 2016). In contrast, Grove et al. and Deng et al. attributed the myelination failure primarily to the
303 inability of SCs to differentiate into myelinating SCs (Deng et al., 2017; Grove et al., 2017).
304 Deng et al., however, disagreed with our view about the role of YAP/TAZ in myelin
305 maintenance of adult nerves (Deng et al., 2017; Grove et al., 2017). These disagreements
306 motivated the present study, which investigated YAP/TAZ expression in adult SCs after nerve
307 injury and their contribution to nerve regeneration. We found that YAP/TAZ dramatically
308 disappear and reappear in SCs after nerve injury, and this loss and recovery of YAP/TAZ in SCs
309 are spatiotemporally correlated with degeneration and regeneration of axons. We also found that

310 SCs lacking YAP/TAZ proliferate and wrap around regenerated axons normally, but then fail to
311 remyelinate them. These findings have several important implications for YAP/TAZ function in
312 mature SCs.

313

314 Using antibodies specifically immunolabeling YAP or YAP/TAZ, we found dramatic down- and
315 upregulation of both nuclear and cytoplasmic YAP/TAZ in SCs after nerve injury.

316 Immunohistochemical identification of SC-selective YAP/TAZ was essential for detecting
317 spatiotemporal regulation of YAP/TAZ. Indeed, we were only able to detect YAP/TAZ
318 downregulation on Western blots when we used lysates prepared from nerves extensively
319 perfused with saline, and from which the epi- and perineurium had been carefully removed. This
320 procedure probably succeeded because it minimized the amount of YAP/TAZ present in cells
321 other than SCs. Careful attention to YAP/TAZ expression in cells other than SCs will help to
322 resolve inconsistencies in earlier studies of YAP/TAZ expression in peripheral nerve.

323

324 YAP/TAZ are located in the nuclei of developing SCs, where they promote proliferation and
325 differentiation (Poitelon et al., 2016; Deng et al., 2017; Grove et al., 2017). They are also nuclear
326 in adult SCs that maintain the myelin sheath (Grove et al., 2017) and that proliferate abnormally
327 (Wu et al., 2018). It was therefore particularly intriguing to find that YAP/TAZ become
328 undetectable in denervated SCs and that SCs lacking YAP/TAZ proliferate normally. YAP/TAZ
329 disappeared from SCs, upon axon degeneration in both crushed and transected nerves. They
330 reappeared in SCs in crushed nerve concomitant with regenerating axons, but not in transected
331 nerve lacking axons, suggesting that YAP/TAZ expression in SCs is dependent on axons. It is
332 also notable that YAP/TAZ appeared unchanged at 1 dpi, but had dramatically disappeared at 3
333 dpi, when axon degeneration was well underway (Beirowski et al., 2005; Gomez-Sanchez et al.,
334 2015; Jang et al., 2016) and denervated SCs had lost contact with axons. Furthermore, SCs that
335 upregulated YAP/TAZ after 3 dpi were associated with regenerating axons large enough to be
336 myelinated. These results are in consistent with our earlier findings of selective expression of
337 YAP/TAZ in myelin-forming SCs (Grove et al., 2017), implying that direct SC-axon contact
338 probably regulate YAP/TAZ down- and upregulation after nerve injury.

339

340 We were surprised to find that SC proliferation proceeds normally in *Yap/Taz* iDKO nerves after
341 injury. Proliferation of mature SCs after injury is therefore due to a YAP/TAZ-independent
342 mechanism, in contrast to the proliferation of developing SCs, which is markedly reduced by
343 YAP/TAZ inactivation (Clemence et al., 1989; Grove et al., 2017). This result is consistent with
344 the notion that the mechanism for SC proliferation during development differs from that for
345 proliferation after injury (Atanasoski et al., 2001; Atanasoski et al., 2008). However, our finding
346 does not indicate that YAP/TAZ are unable to stimulate proliferation of mature SCs. Abnormally
347 high levels of YAP have been shown to elicit excessive SC proliferation in Merlin mutants after
348 nerve injury (Mindos et al., 2017), and YAP/TAZ overexpression induced by LATS1/2
349 inactivation has been shown to induce tumorigenic SC proliferation in adult nerves (Wu et al.,
350 2018). These observations, together with our own, indicate that YAP/TAZ are not normally
351 involved in injury-elicited SC proliferation, but that, if abnormally overexpressed, they can
352 stimulate vigorous SC proliferation. It is also noteworthy that YAP/TAZ inactivation markedly
353 reduces, but does not completely prevent, proliferation of developing SCs (Deng et al., 2017;
354 Grove et al., 2017). We suggest, therefore, that YAP/TAZ are potent stimulants of SC
355 proliferation, but not an absolute requirement.

356
357 Tumorigenic proliferation of adult SCs associated with abnormally increased YAP/TAZ levels
358 (Wu et al., 2018) suggests the importance of maintaining proper levels of YAP/TAZ, but it does
359 not explain why YAP/TAZ are almost completely lost, rather than reduced, in denervated SCs.
360 We previously demonstrated that inducible deletion of YAP/TAZ elicits SC demyelination in
361 adult intact nerve (Grove et al., 2017). If YAP/TAZ indeed maintain myelination and act by
362 promoting transcription of *Krox20* and other myelin genes, then sustaining YAP/TAZ would
363 counteract demyelination and dedifferentiation of SCs after injury. Conversely, their absence
364 would promote downregulation of myelin genes, facilitating demyelination and formation of
365 repair SCs. In accordance with these ideas, transcription of *Krox 20* and other myelin genes
366 remains robust in SCs up until 2 dpi, but is downregulated by 3 dpi (Arthur-Farraj et al., 2017),
367 when we observed dramatic disappearance of YAP/TAZ. This timing suggests that YAP/TAZ
368 protein downregulation leads to *Krox 20* mRNA downregulation, suppressing expression of
369 myelin proteins in de-differentiating Schwann cells. Complete loss of both nuclear and
370 cytoplasmic YAP/TAZ could therefore imply that active regulatory mechanisms completely

371 inactivate YAP/TAZ after injury. In support of this notion, in mutant mice lacking Merlin, YAP
372 is abnormally upregulated in SCs after nerve injury, impairing SC de-differentiation (Mindos et
373 al., 2017). This YAP upregulation suggests that one role of Merlin is to downregulate YAP in
374 SCs and that YAP/TAZ expression in SCs is likely under active, presumably axon-dependent,
375 regulation in both intact and injured mature nerves. This postulation of axon-dependent
376 regulation of YAP/TAZ emphasizes that YAP/TAZ play a passive role in Wallerian degeneration,
377 predicting that SCs do not require YAP/TAZ to dedifferentiate, proliferate, or transdifferentiate
378 to repair SCs. Indeed, we found that these processes proceed normally in *Yap/Taz* iDKO mice.
379
380 iDKO SCs are capable of wrapping around large diameter single axons but fail to initiate
381 remyelination, which recapitulates the developmental phenotype of these mutant mice (Deng et
382 al., 2017; Grove et al., 2017). For at least two reasons remyelination failure is highly unlikely to
383 be due to poor physiological conditions of iDKO mice that die ~14 days after injury. First, axons
384 regenerate normally in iDKO, which is unlikely if SCs are selectively vulnerable to poor
385 physiological condition. Furthermore, iDKO SCs proliferate and trans-differentiate to repair-SCs
386 normally. iDKO SCs also downregulate c-Jun to prepare for remyelination, whereas they
387 maintain a higher level of Oct 6 than WT SCs, consistent with the failure of iDKO SCs to
388 upregulate Krox 20 and MBP. Second, iDKO SCs wrap around individual axons, but fail to
389 myelinate them, indicating that they proceed to the promyelination stage but no further.
390 Therefore, one would have to postulate that the poor physiological condition of iDKO mice has a
391 very specific effect on a particular remyelination stage, which we find unlikely.
392
393 iDKO SCs fail to upregulate Krox 20. Krox 20 is widely accepted as the key transcription factor
394 promoting peripheral myelination. This is largely believed to be the case after injury (Brugger et
395 al., 2017), although its role in remyelination has never been explicitly demonstrated. Other
396 pathways can also promote upregulation of certain myelin proteins and lipids independently of
397 Krox 20 (Domenech-Estevéz et al., 2016), and numerous other factors, both positive and
398 negative regulators, mediate peripheral myelination (Jessen and Mirsky, 2008; Herbert and
399 Monk, 2017). Therefore, it is conceivable that the lack of Krox 20 in iDKO is a consequence
400 rather than a cause of impaired remyelination. However, several considerations make it highly
401 unlikely. First, we and others demonstrated that YAP/TAZ-TEAD1 complex directly binds to the

402 cis-acting regulatory sequence of Krox 20 designated as the Myelinating Schwann cell Element
403 (MSE) to upregulate Krox 20 during developmental myelination (Lopez-Anido et al., 2016;
404 Grove et al., 2017). Second, we showed that YAP/TAZ-TEAD1 also bind to Krox 20 MSE in
405 adult nerve, suggesting direct regulation of Krox 20 by YAP/TAZ in mature SCs (Grove et al.,
406 2017). Third, Oct 6, which induces upregulation of Krox 20, together with other TFs, is
407 upregulated in iDKO after nerve injury, as in WT (Figure 4H, 9G). This finding suggests that
408 remyelination in iDKO is blocked at the step of Krox 20 upregulation. Indeed, we and others
409 have shown that iDKO SCs are arrested at the promyelination stage during development (Deng
410 et al., 2017; Grove et al., 2017), and we found that, similarly after nerve injury, iDKO SCs
411 proceed to the promyelination stage but fail to upregulate Krox 20 and initiate myelin formation.
412

413 YAP upregulation in SCs lacking Merlin has recently been reported to decrease the regeneration-
414 promoting ability of repair SCs, which prevents axon regeneration in Merlin mutants (Mindos et
415 al., 2017). This study implicates YAP as an inhibitor of axon regeneration. Our study suggests
416 that this inhibition is dose- and context-dependent. We observed that repair SCs rapidly
417 upregulate both YAP and TAZ as axons regenerate and that expression persists as regeneration
418 continues. We also found that axon regeneration is as robust in *Taz* iKO and *Yap/Taz* iDKO as in
419 WT, but not noticeably enhanced. Given that YAP is not compensatorily upregulated in *Taz* iKO
420 (Figure 8A), these results suggest that at least normal levels of YAP do not prevent axon
421 regeneration. However, overly robust upregulation of YAP, presumably as in Merlin mutants
422 (Mindos et al., 2017), may severely compromise axon regeneration because excessive levels of
423 YAP/TAZ alter the growth-promoting ability of SCs and/or cause their tumorigenic proliferation.
424

425 The present study, together with earlier work, strongly suggests that the levels of YAP/TAZ may
426 be a critical determinant of their function in adult SCs. Optimal levels of YAP/TAZ promote
427 myelin formation, maintenance and remyelination, whereas their absence promotes
428 demyelination. In contrast, overly excessive levels of YAP/TAZ promote SC proliferation.
429 Additional efforts to confirm this notion and to understand the presumably axon-dependent
430 mechanisms that tightly regulate nuclear levels, thus transcriptional activity, of YAP/TAZ in SCs
431 may generate new strategies for peripheral nerve repair.

432

433 **MATERIALS AND METHODS**

434

Reagent type (species) or resource	Designation	Source or Reference	Identifiers	Additional Information
Strain, strain background (<i>Mus musculus</i>)	C57Bl/6	Jackson Laboratory	Stock #: 000664; RRID:IMSR JAX:000664	
Genetic reagent (<i>M. musculus</i>)	<i>Plp1-Cre-ERT2</i>		MGI:2663093	(Leone et al., 2003)
Antibody	anti-Yap/Taz (rabbit monoclonal)	Cell Signaling Technology	D24E4, #8418 RRID:AB_10950494	IHC 1:200 Western 1:1000
Antibody	anti-SCG10 (rabbit monoclonal)	Novus Biologicals	NBP1-49461 RRID:AB_10011569	IHC 1:5000
Antibody	anti-Yap (rabbit monoclonal)	Cell Signaling Technology	D8H1X, #14074 RRID:AB_2650491	IHC 1:200
Antibody	anti-Sox10 (goat polyclonal)	R&D Systems	#AF-2864 RRID:AB_442208	IHC 1:100
Antibody	anti-Sox10 (rabbit monoclonal)	Abcam	EPR4007, #ab155279 RRID:AB_2650603	IHC 1:250

Antibody	anti-Egr2 (rabbit polyclonal)	Professor Dies Meijer, University of Edinburgh		IHC 1:4000
Antibody	anti-Oct6 (rabbit monoclonal)	Abcam	EP5421, #ab126746 RRID:AB_11130256	WB 1:1000
Antibody	anti-Oct6 (rabbit polyclonal)	Abcam	#ab31766 RRID:AB_776899	IHC 1:800
Antibody	anti-c-Jun (mouse monoclonal)	BD Transduction Laboratories	#610326 RRID:AB_397716	IHC 1:500
Antibody	anti-c-Jun (rabbit monoclonal)	Cell Signaling Technology	60A8, #9165 RRID:AB_2130165	WB 1:1000
Antibody	anti-pS63-c-Jun (rabbit polyclonal)	Cell Signaling Technology	#9261 RRID:AB_2130162	IHC 1:100
Antibody	anti-Ki67 (rabbit polyclonal)	Abcam	#ab15580 RRID:AB_443209	IHC 1:200
Antibody	anti-p75NGFR (goat polyclonal)	Neuromics	#GT15057 RRID:AB_2737189	IHC 1:400
Antibody	anti-Tubulin β 3 (rabbit polyclonal)	Biolegend	#802001 RRID:AB_2564645	IHC 1:1000
Antibody	IRDye-680 (goat anti-mouse)	LI-COR	#926-32220 RRID:AB_621840	WB 1:15,000
Antibody	HRP-Goat anti-mouse secondary antibody	Jackson ImmunoResearch	#715-035-150 RRID:AB_2340770	WB 1:12,000
Antibody	HRP-Goat anti-rabbit secondary antibody	Jackson ImmunoResearch	#115-055-062 RRID:AB_2338533	WB 1:12,000

Chemical compound, drug	Araldite 6005	EMS	#10920	
Chemical compound, drug	DDSA	EMS	#13710	
Chemical compound, drug	DBP	EMS	#13101	
Chemical compound, drug	BDMA	EMS	#11400-25	
other	Coated grids (100 mesh)	EMS	#FF100-Cu	
Chemical compound, drug	Osmium tetroxide (4% solution)	EMS	#19170	
Chemical compound, drug	Lead nitrate	EMS	#17900	
Chemical compound, drug	Sodium citrate	EMS	#21140	
Chemical compound, drug	Uranyl acetate	EMS	#22400	
Chemical compound, drug	Sodium borate	EMS	#21130	
Chemical compound, drug	Toluidine blue	EMS	#22050	
Chemical compound,	Paraformaldehyde	Sigma-Aldrich	#158127	

drug				
Commercial assay or kit	Click-It EdU Alexa Fluor 594 kit	ThermoFisher Scientific	#C10339	
Chemical compound, drug	EdU	ThermoFisher Scientific	#E10187	
Chemical compound, drug	Tamoxifen	Sigma-Aldrich	#T5648	
other	DAPI stain	Invitrogen	#D1306	IHC 1:250
Antibody	Alexa 488, 568 or 647 secondaries	Jackson ImmunoResearch		IHC 1:250 to 1:1000
software, algorithm	Image Studio Lite	LI-COR, Inc		
software, algorithm	Prism	GraphPad Software, Inc		
software, algorithm	Stata	StataCorp LP		Mann-Whitney test

435

436 **Animals**

437 All surgical procedures and animal maintenance complied with the National Institute of Health
438 guidelines regarding the care and use of experimental animals and were approved by the
439 Institutional Animal Care and Use Committee of Temple University, Philadelphia, PA, USA
440 (Protocol 4920). Both male and female mice were used in all experiments, and were maintained
441 on the C57BL/6 background. *Plp1-creERT2; Yap^{fl/fl}; Taz^{fl/fl}*, *Plp1-creERT2; Yap^{+/+}; Taz^{fl/fl}*, *Mpz-*
442 *cre;Yap^{fl/fl}* and *Mpz-cre; Taz^{fl/fl}* mice used in this study were generated and genotyped as
443 described previously (Grove et al., 2017). C57BL/6 mice were used for immunohistochemical
444 analysis of YAP/TAZ.

445

446 **Tamoxifen administration**

447 Tamoxifen was injected into 6-8 week old *Yap/Taz* iDKO or *Taz* iKO mice as previously
448 described (Grove and Brophy, 2014). A 10 mg/ml solution of tamoxifen was made in 10:1
449 sunflower oil: 100% ethanol. This solution was injected intraperitoneally at a concentration of 0.2
450 mg/g body weight. Injection was once daily for 5 days, followed by a 2 day break, then once
451 daily for 5 consecutive days.

452

453 **Nerve crush or transection**

454 Sciatic nerves of right hindlimbs were crushed or transected 24 h after the final tamoxifen
455 injection, using standard protocols (Son and Thompson, 1995). Briefly, a small skin incision was
456 made in the posterior thigh and calf of the animals anesthetized by isoflurane. For crush, the
457 sciatic nerve was crushed with a fine forceps (#5) for 10 seconds (3X) adjacent to the sciatic
458 notch. The crush site was marked using charcoal-coated forceps, and the wound was closed. For
459 transection, the exposed sciatic nerve was ligated at two directly adjacent sites, then cut with
460 iridectomy scissors between the ligated sites. Ligated proximal and distal nerve endings were
461 then sewn to adjacent muscle to prevent regeneration of axons from the proximal to distal nerve
462 stumps. To identify proliferating Schwann cells, we intraperitoneally injected EdU (80 µg/g)
463 eighty minutes before killing mice, as previously described (Grove et al., 2017).

464

465 **Western blotting**

466 Mice were perfused with PBS, sciatic nerves removed, and epineurium and perineurium
467 carefully stripped from the nerves. Western blotting followed the same procedure described
468 previously (Grove et al., 2017), except for IRDye 680RD goat anti-mouse IgG (LiCor #926-
469 68070; 1:5,000). Image Studio Lite (LI-COR Biosciences) was used for quantifying protein
470 expression.

471

472 **Immunohistochemistry**

473 Sciatic nerves were removed, and immediately fixed in 4% paraformaldehyde in PBS for 1 hour
474 on ice. Nerves were washed 3 times in PBS, then stored in 15% sucrose in PBS overnight at 4°C
475 for cryoprotection. Nerves were frozen-embedded in cryoprotectant medium (Thermo Fisher
476 Scientific, Waltham, MA) in isomethylbutane at -80°C. 7-10 µm sections from the nerves were
477 cut using a cryostat (Leica Microsystems, Germany) and collected directly onto glass slides. For

478 immunolabeling, nerve sections were rehydrated in PBS, permeabilized in 0.5% Triton/PBS for
479 20 min, washed with PBS, then blocked in 2% bovine serum albumin (BSA) in PBS for 1hr.
480 Sections were incubated with primary antibodies in blocking buffer overnight at 4°C in a
481 hydrated chamber, washed with PBS, and incubated with secondary antibodies in blocking buffer
482 for 2hrs at room temperature. Sections were washed with PBS, stained with DAPI for 10 min,
483 and mounted with Vectashield mounting medium (Vector Labs, Burlingame, CA). Nerve
484 sections were incubated with antibodies previously described (Grove et al., 2017), except for the
485 following: rabbit anti-Krox20 (kind gift from Professor Dies Meijer, Edinburgh, UK; 1:4000),
486 rabbit anti-Yap (Cell Signaling #14074; 1:200), rabbit anti-SCG10 (Novus Biologicals #49461;
487 1:5000), goat anti-Sox10 (Santa Cruz #sc-17342; 1:200), goat anti-Sox10 (R&D Systems #AF-
488 2864; 1:100), goat anti-p75 (Neuromics #GT15057; 1:400), rabbit anti-Ki67 (Abcam #ab15580;
489 1:1000), mouse anti-Tubulin β 3 (clone Tuj1, Covance #MMS-435P; 1:1000), mouse anti-cJun
490 (BD Biosciences #610326; 1:500), rabbit anti-cJun (CST #9165; 1:500), rabbit anti-phospho-
491 cJun (CST #9261; 1:100).

492

493 **Electron microscopy, histology and morphometry**

494 Sciatic nerves were removed and immediately fixed in EM buffer, as previously described
495 (Grove et al., 2017). After nerve crush or transection, a 5 mm piece of the nerve was taken
496 immediately distal to the injury site. The proximal end of the section was nicked with a razor
497 blade for orientation during embedding. Fixation was for 2 h at room temperature, followed by
498 overnight at 4°C, with rotation. Post-fixation processing, embedding, cutting, staining and image
499 capture were as previously described. For crushed or transected nerves, 500 nm semi-thin and 70
500 nm ultra-thin transverse sections were cut from the segment 5 mm distal to the crush/transection
501 site.

502

503 For analysis of axon regeneration and remyelination, 7500x TEM sections were examined. This
504 magnification allowed unambiguous identification of basal lamina tubes through which axons
505 regenerate. Multiple non-overlapping images were taken for each section, such that all regions of
506 each section were sampled. Image J was used for image analysis. After counting the total number
507 of basal lamina (BL) tubes per image, we next counted the number of BL tubes in the following
508 categories: contains no axon(s); contains axon(s); contains at least 1 axon > 1 μ m in diameter;

509 contains a single axon $> 1\mu\text{m}$ in diameter; contains a myelinated axon. This procedure enabled
510 us to calculate the percentage of BL tubes in each category. Using an ImageJ G-ratio calculator
511 plug-in, G ratios for each genotype were calculated in 2 different ways: (1) All single large axons
512 were counted, whether or not they were myelinated; (2) Only myelinated axons were counted.

513

514 **Data Analysis**

515 In each experiment, data collection and analysis were performed identically, regardless of mouse
516 genotype. Data are presented as mean \pm SD. Statistical analysis was done using the two-sample
517 Mann-Whitney test for two-group comparisons and analysis of variance (ANOVA) with Tukey's
518 test for multiple comparisons, according to the number of samples and the analysis of mice at
519 multiple ages. Sample sizes were similar to those employed in the field and are indicated in the
520 main text, methods or figure legends. A p-value of 0.05 or less was considered statistically
521 significant.

522

523 **ACKNOWLEDGMENTS**

524 We thank Alan Tessler and members of the Son laboratory for critical reading of the manuscript.
525 We thank Dr. Hyukmin Kim for intraperitoneal injection, Dr. Eric Olson for Yap and Taz floxed
526 mice, Drs. Ueli Suter and Kelly Monk for Plp-creERT2 mice. Plp-creERT2 mice were generated
527 by Dr. Ueli Suter using a patented Cre-ERT2 construct developed by Dr. Pierre Chambon at
528 GIE-CERBM. This paper is dedicated to the memory of Dr. Wesley Thompson who revealed the
529 pivotal roles of terminal Schwann cells in forming and restoring nerve-muscle connection.

530

531 **COMPETING INTERESTS**

532 The authors declare no competing financial interests.

533

534 **FUNDINGS**

535 This work was supported by grants from Shriners Hospitals for Children and NIH NINDS
536 (NS105796 to Y-J.S.).

537

538 **REFERENCES**

- 539 Arthur-Farraj, P. J., Latouche, M., Wilton, D. K., Quintes, S., Chabrol, E., Banerjee, A.,
540 Woodhoo, A., Jenkins, B., Rahman, M., Turmaine, M., Wicher, G. K., Mitter, R.,
541 Greensmith, L., Behrens, A., Raivich, G., Mirsky, R., and Jessen, K. R. (2012). c-Jun
542 reprograms Schwann cells of injured nerves to generate a repair cell essential for
543 regeneration. *Neuron*, 75(4), 633-647. doi:10.1016/j.neuron.2012.06.021
- 544 Arthur-Farraj, P. J., Morgan, C. C., Adamowicz, M., Gomez-Sanchez, J. A., Fazal, S. V.,
545 Beucher, A., Razzaghi, B., Mirsky, R., Jessen, K. R., and Aitman, T. J. (2017). Changes
546 in the Coding and Non-coding Transcriptome and DNA Methylome that Define the
547 Schwann Cell Repair Phenotype after Nerve Injury. *Cell Rep*, 20(11), 2719-2734.
548 doi:10.1016/j.celrep.2017.08.064
- 549 Atanasoski, S., Boentert, M., De Ventura, L., Pohl, H., Baranek, C., Beier, K., Young, P.,
550 Barbacid, M., and Suter, U. (2008). Postnatal Schwann cell proliferation but not
551 myelination is strictly and uniquely dependent on cyclin-dependent kinase 4 (cdk4). *Mol*
552 *Cell Neurosci*, 37(3), 519-527. doi:10.1016/j.mcn.2007.11.005
- 553 Atanasoski, S., Shumas, S., Dickson, C., Scherer, S. S., and Suter, U. (2001). Differential cyclin
554 D1 requirements of proliferating Schwann cells during development and after injury. *Mol*
555 *Cell Neurosci*, 18(6), 581-592. doi:10.1006/mcne.2001.1055
- 556 Beirowski, B., Adalbert, R., Wagner, D., Grumme, D. S., Addicks, K., Ribchester, R. R., and
557 Coleman, M. P. (2005). The progressive nature of Wallerian degeneration in wild-type
558 and slow Wallerian degeneration (WldS) nerves. *BMC Neurosci*, 6, 6. doi:10.1186/1471-
559 2202-6-6
- 560 Clemence, A., Mirsky, R., and Jessen, K. R. (1989). Non-myelin-forming Schwann cells
561 proliferate rapidly during Wallerian degeneration in the rat sciatic nerve. *J Neurocytol*,
562 18(2), 185-192.
- 563 Cotton, J. L., Li, Q., Ma, L., Park, J. S., Wang, J., Ou, J., Zhu, L. J., Ip, Y. T., Johnson, R. L., and
564 Mao, J. (2017). YAP/TAZ and Hedgehog Coordinate Growth and Patterning in
565 Gastrointestinal Mesenchyme. *Dev Cell*, 43(1), 35-47 e34.
566 doi:10.1016/j.devcel.2017.08.019
- 567 Decker, L., Desmarquet-Trin-Dinh, C., Taillebourg, E., Ghislain, J., Vallat, J. M., and Charnay,
568 P. (2006). Peripheral myelin maintenance is a dynamic process requiring constant
569 Krox20 expression. *J Neurosci*, 26(38), 9771-9779. doi:10.1523/JNEUROSCI.0716-
570 06.2006
- 571 Deng, Y., Wu, L. M. N., Bai, S., Zhao, C., Wang, H., Wang, J., Xu, L., Sakabe, M., Zhou, W.,
572 Xin, M., and Lu, Q. R. (2017). A reciprocal regulatory loop between TAZ/YAP and G-
573 protein Galphas regulates Schwann cell proliferation and myelination. *Nat Commun*, 8,
574 15161. doi:10.1038/ncomms15161
- 575 Domenech-Estevez, E., Baloui, H., Meng, X., Zhang, Y., Deinhardt, K., Dupree, J. L., Einheber,
576 S., Chrast, R., and Salzer, J. L. (2016). Akt Regulates Axon Wrapping and Myelin Sheath

- 577 Thickness in the PNS. *J Neurosci*, 36(16), 4506-4521. doi:10.1523/jneurosci.3521-
578 15.2016
- 579 Feltri, M. L., Poitelon, Y., and Previtali, S. C. (2016). How Schwann Cells Sort Axons: New
580 Concepts. *Neuroscientist*, 22(3), 252-265. doi:10.1177/1073858415572361
- 581 Fernando, R. N., Cotter, L., Perrin-Tricaud, C., Berthelot, J., Bartolami, S., Pereira, J. A.,
582 Gonzalez, S., Suter, U., and Tricaud, N. (2016). Optimal myelin elongation relies on
583 YAP activation by axonal growth and inhibition by Crb3/Hippo pathway. *Nat Commun*, 7,
584 12186. doi:10.1038/ncomms12186
- 585 Fex Svenningsen, A., and Dahlin, L. B. (2013). Repair of the Peripheral Nerve-Remyelination that
586 Works. *Brain Sci*, 3(3), 1182-1197. doi:10.3390/brainsci3031182
- 587 Fontana, X., Hristova, M., Da Costa, C., Patodia, S., Thei, L., Makwana, M., Spencer-Dene, B.,
588 Latouche, M., Mirsky, R., Jessen, K. R., Klein, R., Raivich, G., and Behrens, A. (2012).
589 c-Jun in Schwann cells promotes axonal regeneration and motoneuron survival via
590 paracrine signaling. *J Cell Biol*, 198(1), 127-141. doi:10.1083/jcb.201205025
- 591 Frendo, M. E., da Silva, A., Phan, K. D., Riche, S., and Butler, S. J. (2019). The Cofilin/Limk1
592 Pathway Controls the Growth Rate of Both Developing and Regenerating Motor Axons.
593 *J Neurosci*, 39(47), 9316-9327. doi:10.1523/jneurosci.0648-19.2019
- 594 Gaudet, A. D., Popovich, P. G., and Ramer, M. S. (2011). Wallerian degeneration: gaining
595 perspective on inflammatory events after peripheral nerve injury. *Journal of*
596 *neuroinflammation*, 8, 110. doi:10.1186/1742-2094-8-110
- 597 Gomez-Sanchez, J. A., Carty, L., Iruarrizaga-Lejarreta, M., Palomo-Irigoyen, M., Varela-Rey,
598 M., Griffith, M., Hantke, J., Macias-Camara, N., Azkargorta, M., Aurrekoetxea, I., De
599 Juan, V. G., Jefferies, H. B., Aspichueta, P., Elortza, F., Aransay, A. M., Martinez-
600 Chantar, M. L., Baas, F., Mato, J. M., Mirsky, R., Woodhoo, A., and Jessen, K. R. (2015).
601 Schwann cell autophagy, myelinophagy, initiates myelin clearance from injured nerves. *J*
602 *Cell Biol*, 210(1), 153-168. doi:10.1083/jcb.201503019
- 603 Grove, M., and Brophy, P. J. (2014). FAK is required for Schwann cell spreading on immature
604 basal lamina to coordinate the radial sorting of peripheral axons with myelination. *J*
605 *Neurosci*, 34(40), 13422-13434. doi:10.1523/JNEUROSCI.1764-14.2014
- 606 Grove, M., Kim, H., Santerre, M., Krupka, A. J., Han, S. B., Zhai, J., Cho, J. Y., Park, R., Harris,
607 M., Kim, S., Sawaya, B. E., Kang, S. H., Barbe, M. F., Cho, S. H., Lemay, M. A., and
608 Son, Y. J. (2017). YAP/TAZ initiate and maintain Schwann cell myelination. *Elife*, 6.
609 doi:10.7554/eLife.20982
- 610 Herbert, A. L., and Monk, K. R. (2017). Advances in myelinating glial cell development. *Curr*
611 *Opin Neurobiol*, 42, 53-60. doi:10.1016/j.conb.2016.11.003

- 612 Jang, S. Y., Shin, Y. K., Park, S. Y., Park, J. Y., Lee, H. J., Yoo, Y. H., Kim, J. K., and Park, H.
613 T. (2016). Autophagic myelin destruction by Schwann cells during Wallerian
614 degeneration and segmental demyelination. *Glia*, 64(5), 730-742. doi:10.1002/glia.22957
- 615 Jessen, K. R., and Mirsky, R. (2008). Negative regulation of myelination: relevance for
616 development, injury, and demyelinating disease. *Glia*, 56(14), 1552-1565.
617 doi:10.1002/glia.20761
- 618 Jessen, K. R., and Mirsky, R. (2016). The repair Schwann cell and its function in regenerating
619 nerves. *J Physiol*, 594(13), 3521-3531. doi:10.1113/jp270874
- 620 Kang, H., and Lichtman, J. W. (2013). Motor axon regeneration and muscle reinnervation in
621 young adult and aged animals. *J Neurosci*, 33(50), 19480-19491.
622 doi:10.1523/jneurosci.4067-13.2013
- 623 Leone, D. P., Genoud, S., Atanasoski, S., Grausenburger, R., Berger, P., Metzger, D., Macklin,
624 W. B., Chambon, P., and Suter, U. (2003). Tamoxifen-inducible glia-specific Cre mice
625 for somatic mutagenesis in oligodendrocytes and Schwann cells. *Mol Cell Neurosci*,
626 22(4), 430-440.
- 627 Lopez-Anido, C., Poitelon, Y., Gopinath, C., Moran, J. J., Ma, K. H., Law, W. D., Antonellis, A.,
628 Feltri, M. L., and Svaren, J. (2016). Tead1 regulates the expression of Peripheral Myelin
629 Protein 22 during Schwann cell development. *Hum Mol Genet*. doi:10.1093/hmg/ddw158
- 630 Mindos, T., Dun, X. P., North, K., Doddrell, R. D., Schulz, A., Edwards, P., Russell, J., Gray, B.,
631 Roberts, S. L., Shivane, A., Mortimer, G., Pirie, M., Zhang, N., Pan, D., Morrison, H.,
632 and Parkinson, D. B. (2017). Merlin controls the repair capacity of Schwann cells after
633 injury by regulating Hippo/YAP activity. *J Cell Biol*, 216(2), 495-510.
634 doi:10.1083/jcb.201606052
- 635 Mogha, A., Harty, B. L., Carlin, D., Joseph, J., Sanchez, N. E., Suter, U., Piao, X., Cavalli, V.,
636 and Monk, K. R. (2016). Gpr126/Adgrg6 Has Schwann Cell Autonomous and
637 Nonautonomous Functions in Peripheral Nerve Injury and Repair. *J Neurosci*, 36(49),
638 12351-12367. doi:10.1523/JNEUROSCI.3854-15.2016
- 639 Moon, S., Yeon Park, S., and Woo Park, H. (2018). Regulation of the Hippo pathway in cancer
640 biology. *Cell Mol Life Sci*, 75(13), 2303-2319. doi:10.1007/s00018-018-2804-1
- 641 Parkinson, D. B., Bhaskaran, A., Arthur-Farraj, P., Noon, L. A., Woodhoo, A., Lloyd, A. C.,
642 Feltri, M. L., Wrabetz, L., Behrens, A., Mirsky, R., and Jessen, K. R. (2008). c-Jun is a
643 negative regulator of myelination. *J Cell Biol*, 181(4), 625-637.
644 doi:10.1083/jcb.200803013
- 645 Poitelon, Y., Lopez-Anido, C., Catignas, K., Berti, C., Palmisano, M., Williamson, C., Ameroso,
646 D., Abiko, K., Hwang, Y., Gregorieff, A., Wrana, J. L., Asmani, M., Zhao, R., Sim, F. J.,
647 Wrabetz, L., Svaren, J., and Feltri, M. L. (2016). YAP and TAZ control peripheral
648 myelination and the expression of laminin receptors in Schwann cells. *Nat Neurosci*,
649 19(7), 879-887. doi:10.1038/nn.4316

- 650 Quintes, S., Brinkmann, B. G., Ebert, M., Frob, F., Kungl, T., Arlt, F. A., Tarabykin, V.,
651 Huylebroeck, D., Meijer, D., Suter, U., Wegner, M., Sereda, M. W., and Nave, K. A.
652 (2016). Zeb2 is essential for Schwann cell differentiation, myelination and nerve repair.
653 *Nat Neurosci*. doi:10.1038/nn.4321
- 654 Scheib, J., and Hoke, A. (2013). Advances in peripheral nerve regeneration. *Nat Rev Neurol*,
655 9(12), 668-676. doi:10.1038/nrneurol.2013.227
- 656 Scherer, S. S., Wang, D. Y., Kuhn, R., Lemke, G., Wrabetz, L., and Kamholz, J. (1994). Axons
657 regulate Schwann cell expression of the POU transcription factor SCIP. *J Neurosci*, 14(4),
658 1930-1942.
- 659 Shin, J. E., Geisler, S., and DiAntonio, A. (2014). Dynamic regulation of SCG10 in regenerating
660 axons after injury. *Exp Neurol*, 252, 1-11. doi:10.1016/j.expneurol.2013.11.007
- 661 Son, Y.-J., and Thompson, W. J. (1995). Schwann cell processes guide regeneration of
662 peripheral axons. *Neuron*, 14, 125-132.
- 663 Stassart, R. M., Fledrich, R., Velanac, V., Brinkmann, B. G., Schwab, M. H., Meijer, D., Sereda,
664 M. W., and Nave, K. A. (2013). A role for Schwann cell-derived neuregulin-1 in
665 remyelination. *Nat Neurosci*, 16(1), 48-54. doi:10.1038/nn.3281
- 666 Stierli, S., Napoli, I., White, I. J., Cattin, A. L., Monteza Cabrejos, A., Garcia Calavia, N.,
667 Malong, L., Ribeiro, S., Nihouarn, J., Williams, R., Young, K. M., Richardson, W. D.,
668 and Lloyd, A. C. (2018). The regulation of the homeostasis and regeneration of
669 peripheral nerve is distinct from the CNS and independent of a stem cell population.
670 *Development*, 145(24). doi:10.1242/dev.170316
- 671 Topilko, P., Schneider-Maunoury, S., Levi, G., Baron-Van Evercooren, A., Chennoufi, A. B.,
672 Seitanidou, T., Babinet, C., and Charnay, P. (1994). Krox-20 controls myelination in the
673 peripheral nervous system. *Nature*, 371(6500), 796-799. doi:10.1038/371796a0
- 674 Tricaud, N., and Park, H. T. (2017). Wallerian demyelination: chronicle of a cellular cataclysm.
675 *Cell Mol Life Sci*, 74(22), 4049-4057. doi:10.1007/s00018-017-2565-2
- 676 Varelas, X. (2014). The Hippo pathway effectors TAZ and YAP in development, homeostasis
677 and disease. *Development*, 141(8), 1614-1626. doi:10.1242/dev.102376
- 678 von Gise, A., Lin, Z., Schlegelmilch, K., Honor, L. B., Pan, G. M., Buck, J. N., Ma, Q., Ishiwata,
679 T., Zhou, B., Camargo, F. D., and Pu, W. T. (2012). YAP1, the nuclear target of Hippo
680 signaling, stimulates heart growth through cardiomyocyte proliferation but not
681 hypertrophy. *Proc Natl Acad Sci U S A*, 109(7), 2394-2399.
682 doi:10.1073/pnas.1116136109
- 683 Wang, J., Liu, S., Heallen, T., and Martin, J. F. (2018). The Hippo pathway in the heart: pivotal
684 roles in development, disease, and regeneration. *Nat Rev Cardiol*, 15(11), 672-684.
685 doi:10.1038/s41569-018-0063-3

- 686 Wu, L. M., Wang, J., Conidi, A., Zhao, C., Wang, H., Ford, Z., Zhang, L., Zweier, C., Ayee, B.
687 G., Maurel, P., Zwijsen, A., Chan, J. R., Jankowski, M. P., Huylebroeck, D., and Lu, Q.
688 R. (2016). Zeb2 recruits HDAC-NuRD to inhibit Notch and controls Schwann cell
689 differentiation and remyelination. *Nat Neurosci*. doi:10.1038/nn.4322
- 690 Wu, L. M. N., Deng, Y., Wang, J., Zhao, C., Wang, J., Rao, R., Xu, L., Zhou, W., Choi, K.,
691 Rizvi, T. A., Remke, M., Rubin, J. B., Johnson, R. L., Carroll, T. J., Stemmer-
692 Rachamimov, A. O., Wu, J., Zheng, Y., Xin, M., Ratner, N., and Lu, Q. R. (2018).
693 Programming of Schwann Cells by Lats1/2-TAZ/YAP Signaling Drives Malignant
694 Peripheral Nerve Sheath Tumorigenesis. *Cancer Cell*, 33(2), 292-308 e297.
695 doi:10.1016/j.ccell.2018.01.005
- 696 Xin, M., Kim, Y., Sutherland, L. B., Murakami, M., Qi, X., McAnally, J., Porrello, E. R.,
697 Mahmoud, A. I., Tan, W., Shelton, J. M., Richardson, J. A., Sadek, H. A., Bassel-Duby,
698 R., and Olson, E. N. (2013). Hippo pathway effector Yap promotes cardiac regeneration.
699 *Proc Natl Acad Sci U S A*, 110(34), 13839-13844. doi:10.1073/pnas.1313192110
- 700 Yu, F. X., Zhao, B., and Guan, K. L. (2015). Hippo Pathway in Organ Size Control, Tissue
701 Homeostasis, and Cancer. *Cell*, 163(4), 811-828. doi:10.1016/j.cell.2015.10.044
- 702 Zanconato, F., Cordenonsi, M., and Piccolo, S. (2016). YAP/TAZ at the Roots of Cancer.
703 *Cancer Cell*, 29(6), 783-803. doi:10.1016/j.ccell.2016.05.005
- 704 Zhang, H., Deo, M., Thompson, R. C., Uhler, M. D., and Turner, D. L. (2012). Negative
705 regulation of Yap during neuronal differentiation. *Dev Biol*, 361(1), 103-115.
706 doi:10.1016/j.ydbio.2011.10.017

707
708

709 **FIGURE LEGENDS**

710 **Figure 1. Loss and recovery of YAP/TAZ in Schwann cells after sciatic nerve crush**

711 YAP/TAZ expression in crushed sciatic nerves of adult mice, shown by IHC (A, B) and Western
712 blotting (C). Axons and Schwann cell (SC) nuclei are marked by neurofilament (NF) or Sox10,
713 respectively. (A) A surgery schematic for nerve crush, which permits regeneration of axons into
714 the distal nerve stump, illustrated by a low-magnification, longitudinal section of a sciatic nerve
715 at 12 dpi, immunostained for YAP and TAZ. (B) Dramatic loss of YAP/TAZ in SC nuclei by 3
716 dpi, concomitant with axon degeneration, followed by upregulation of YAP/TAZ after 6 dpi,
717 concomitant with axon regeneration. Right-most panels: zoomed area of merged images, as
718 indicated, showing nuclear expression of YAP/TAZ in SCs associated with large diameter axons,
719 before and after injury. Arrows point to large diameter axons in distal nerves before injury or 1
720 dpi, associated with YAP/TAZ+ SC nuclei. Arrowheads point to regenerating axons. Note that

721 SC nuclei associated with a thin regenerating axon at 3 dpi do not express nuclear YAP/TAZ, but
722 those in contact with a large diameter axon after 6 dpi do. Scale bars; 500 μ m (A), 20 μ m (B). (C)
723 Western blotting of intact and crushed nerve lysates, showing loss of YAP and TAZ by 3 dpi,
724 followed by full recovery of TAZ but not YAP by 12 dpi. Quantification of Western blots: n =
725 3-5 mice per experiment. ns = not significant, 2-way ANOVA. YAP: 1 dpi intact vs 1dpi crushed,
726 P = 0.9991; 1 dpi crushed vs 3 dpi crushed, ****P < 0.0001; 1 dpi crushed vs 6 dpi crushed,
727 ***P = 0.0009; 1 dpi crushed vs 12 dpi crushed, ****P < 0.0001; 3 dpi intact vs 3 dpi crushed,
728 ****P < 0.0001; 3 dpi crushed vs 6 dpi crushed, P = 0.0652; 3 dpi crushed vs 12 dpi crushed, P =
729 0.3479; 6 dpi intact vs 6 dpi crushed, ***P = 0.0009; 6 dpi crushed vs 12 dpi crushed, **P =
730 0.0018; 12 dpi intact vs 12 dpi crushed, ****P < 0.0001. TAZ: 1 dpi intact vs 1 dpi crushed, P =
731 0.9909; 1 dpi crushed vs 3 dpi crushed, ****P < 0.0001; 1 dpi crushed vs 6 dpi crushed, P =
732 0.6855; 1 dpi crushed vs 12 dpi crushed, P = 0.9692; 3 dpi intact vs 3 dpi crushed, ****P <
733 0.0001; 3 dpi crushed vs 6 dpi crushed, ****P < 0.0001; 3 dpi crushed vs 12 dpi crushed, ****P
734 < 0.0001; 6 dpi intact vs 6 dpi crushed, P = 0.9828; 6 dpi crushed vs 12 dpi crushed, P = 0.9810;
735 12 dpi intact vs 12 dpi crushed, P > 0.9999.

736

737 The following figure supplements are available for Figure 1.

738 **Figure 1-figure supplement 1**

739 **Additional assessment of YAP expression in Schwann cells after nerve injury**

740 (A) Validation of a YAP-specific antibody. The antibody labels perineurial cells but not SC
741 nuclei in intact sciatic nerves of *Yap* cKO (*Mpz-Cre; Yap^{fl/fl}; Taz^{+/+}*, Upper panel), whereas it
742 labels SC nuclei in *Taz* cKO mice (*Mpz-Cre; Yap^{+/+}; Taz^{fl/fl}*, Bottom panel). (B) Longitudinal
743 sections of crushed nerves, showing loss of YAP from SC nuclei in distal nerves by 3 dpi,
744 followed by re-upregulation at or after 6 dpi. Scale bars = 15 μ m (A, B).

745

746 **Figure 1- source data 1**

747 **Source files for Yap and Taz Western graphs**

748 This zip archive contains the raw data for WT and iDKO used for the quantitative analysis
749 shown in Figure 1C. Data are in GraphPad Prism files, as indicated.

750

751 **Figure 1-source data 2**

752 **Time course of YAP and TAZ protein expression in WT nerves after sciatic nerve crush.**

753 Uncropped Western blots of images used to make Figure 1C. Individually processed samples
754 from 6 mice at 3 dpi, 5 mice at 12 dpi, and 3 mice at both 1 dpi and 6 dpi are shown and used for
755 quantification. X.....X denotes the line along which membranes were cut prior to probing with
756 anti-beta actin antibody. Two exposures of anti-YAP/TAZ blot are shown.

757

758 **Figure 2. YAP/TAZ expression in Schwann cells after sciatic nerve transection**

759 (A, B, C) YAP/TAZ expression in transected sciatic nerves of adult mice. Axons and Schwann
760 cell (SC) nuclei are marked by neurofilament (NF) or Sox10, respectively. (A) A surgery
761 schematic for nerve transection illustrated by a low-magnification, longitudinal section of a
762 sciatic nerve at 12 dpi, immunostained for YAP and TAZ. Axon regeneration into the distal
763 nerve stump was prevented by ligating the transected nerve stumps. (B) Complete loss of
764 YAP/TAZ in SC nuclei at and after 3 dpi, concomitant with axon degeneration. Right-most
765 panels: zoomed area of merged images, as indicated, showing that SCs do not upregulate
766 YAP/TAZ in the absence of regenerating axons. (C) Cytoplasmic loss of phosphorylated YAP
767 (p-YAP) in SCs of transected nerve. p-YAP was undetectable in axotomized SCs at 12 dpi. (D)
768 Upregulation of p-YAP in SCs of crushed nerve. p-YAP was detectable in innervated SCs at 12
769 dpi. Right-most panel: zoomed area of merged image, showing a SC nucleus exhibiting
770 perinuclear cytoplasmic p-YAP. Scale bars; 500µm (A), 20µm (B-D).

771

772 **Figure 3. YAP/TAZ are dispensable for Schwann cell proliferation after axotomy**

773 (A) Schematic showing timeline of tamoxifen injection, sciatic nerve transection and sacrifice of
774 adult WT or Yap/Taz iDKO. (B) Longitudinal sections of intact sciatic nerves showing efficient
775 deletion of YAP/TAZ in iDKO. SC nuclei are marked by Sox10 (red). All cell nuclei are marked
776 by DAPI (blue). (C) Longitudinal sections of transected nerves of WT or iDKO showing SCs in
777 S-phase of the cell cycle marked by EdU (green). (D) Longitudinal sections of transected nerves
778 of WT or iDKO showing proliferating SCs marked by Ki67 (green). (E) Transverse sections of
779 transected nerves of WT or iDKO showing SCs marked by Sox10 (red). (F) Quantification of
780 SCs expressing nuclear YAP/TAZ in intact sciatic nerves of WT or iDKO. n = 3 mice per
781 genotype, *P = 0.0495, Mann-Whitney. (G) Quantification of EdU+ SCs in transected nerves of
782 WT or iDKO. n = 3 mice per genotype, *P = 0.0463, Mann-Whitney. (H) Quantification of

783 Ki67+ proliferating SCs in transected nerves of WT or iDKO. n = 3 mice per genotype, ns, not
784 significant, P = 0.5127, Mann-Whitney. (I) Quantification of Sox10+ SCs in transected nerves of
785 WT or iDKO. n = 3 mice per genotype. ns, not significant, P = 0.8273, Mann-Whitney. Scale
786 bars = 30µm (B-E).

787

788 The following figure supplements are available for Figure 3.

789 **Figure 3-figure supplement 1**

790 **No Schwann cell proliferation or death in intact nerves of *Yap/Taz* iDKO at 12 dpi**

791 (A) Schematic showing experimental procedures analyzing contralateral intact nerves of WT or
792 iDKO at 12 dpi. (B) Longitudinal sections showing absence of EdU+ SCs in S-phase in intact
793 nerves of iDKO, as in WT. Asterisks denote EdU+ cells that are not SCs, as indicated by their
794 lack of Sox10. (C) Longitudinal sections of contralateral intact nerves, showing absence of
795 apoptotic SCs identified by FITC-dUTP incorporation in iDKO, as in WT. (D) Transverse
796 sections of intact nerves, showing similar numbers of SCs (marked by Sox10) in intact nerves of
797 WT and iDKO at 12 dpi. All nuclei are marked by DAPI. (E) Quantification of SCs in intact
798 nerves of WT or iDKO, showing no significant difference. n = 3 mice per genotype. ns, not
799 significant, P = 0.5127, Mann-Whitney. Scale bars = 50µm (B-D).

800

801 **Figure 3- source data 1**

802 **Source files for EdU⁺ SC data**

803 This zip archive contains the IHC images for one WT and one iDKO used for the quantitative
804 analysis shown in Figure 3G. Leica SP8 confocal lif images were processed using Imaris
805 software and saved as tiffs.

806

807 **Figure 3-source data 2**

808 **Source files for Ki67⁺ SC data**

809 This zip archive contains the IHC for one WT and one iDKO used for quantitative analysis
810 shown in Figure 3H. Results and quantitation shown in the Figure used BD #550609 anti-Ki67.
811 These results were confirmed using a second antibody, Abcam #ab15580 anti-Ki67. Images
812 using both antibodies are included in the zip archive, in the indicated folders. Leica SP8 confocal
813 lif images were processed using Imaris software and saved as tiffs.

814

815 **Figure 3- source data 3**

816 **Source files for graphs quantifying Yap/Taz+ SCs, EdU+ SCs, Ki67+ SCs, and total SCs**

817 This zip archive contains the raw data for WT and iDKO used for the quantitative analysis
818 shown in Figures 3F, 3G, 3H and 3I. The data is contained in both a text document and an Excel
819 file, both labeled as Mann Whitney data. These files also contain data for Figures 3-S1, 4, 5, 6, 7,
820 8A and 8-S1E.

821

822 **Figure 3-figure supplement 1- source data 1**

823 **Source files for graph quantifying total SCs**

824 This zip archive contains the raw data for WT and iDKO used for the quantitative analysis
825 shown in Figures 3-S1E. The data is contained in both a text document and an Excel file, both
826 labeled as Mann Whitney data. These files also contain data for Figures 3, 4, 5, 6, 7, 8A and 8-
827 S1E.

828

829 **Figure 4. Schwann cells lacking YAP/TAZ transdifferentiate into repair Schwann cells**

830 Longitudinal sections of transected sciatic nerves of WT and *Yap/Taz* iDKO immunostained by
831 various markers of growth-promoting repair SCs at 5 dpi. SCs are marked by Sox10 (red). (A)
832 Representative sections showing upregulation of c-Jun in iDKO SCs, as in WT SCs. (B)
833 Upregulation of active phospho-S63 c-Jun in iDKO SCs, as in WT. (C) Upregulation of p75 in
834 iDKO SCs, as in WT SCs. (D) Upregulation of Oct-6 in iDKO SCs, as in WT SCs. (E)
835 Quantification of c-Jun+ SCs in WT and iDKO. n = 3 mice per genotype. ns, not significant, P =
836 0.1266, Mann-Whitney. (F) Quantification of pc-Jun+ SCs in WT and iDKO. n = 3 mice per
837 genotype. *P = 0.0495, Mann-Whitney. (G) Quantification of p75+ SCs in WT and iDKO. n = 3
838 mice per genotype. ns, not significant, P = 0.5127, Mann-Whitney. (H) Quantification of Oct-6+
839 SCs in WT and iDKO. n = 3 mice per genotype. ns, not significant, P = 0.8273, Mann-Whitney.
840 Scale bars = 30µm (A-D).

841

842 **Figure 4-source data 1**

843 **Source files for c-Jun⁺ SC data**

844 This zip archive contains the IHC for one WT and one iDKO used for quantitative analysis
845 shown in Figure 4E. Leica SP8 confocal lif images were processed using Imaris software and
846 saved as tiffs.

847

848 **Figure 4- source data 2**

849 **Source files for graphs quantifying c-Jun+ SCs, pc-Jun+ SCs, p75+ SCs, and Oct6+ SCs**

850 This zip archive contains the raw data for WT and iDKO used for the quantitative analysis
851 shown in Figures 4E, 4F, 4G and 4H. The data is contained in both a text document and an Excel
852 file, both labeled as Mann Whitney data. These files also contain data for Figures 3, 3-S1, 5, 6, 7,
853 8A and 8-S1E.

854

855 **Figure 4-source data 3**

856 **Western blotting analysis of repair Schwann cell markers**

857 Uncropped Western blots of images used to make Figure 4-figure supplement 1. Individually
858 processed samples from 2 WT (#656, #625) and 2 iDKO mice (#378, #379) are shown and used
859 for quantification.

860

861 The following figure supplements are available for Figure 4

862 **Figure 4-figure supplement 1**

863 **Western blotting analysis of repair Schwann cell markers**

864 (A) Western blots of lysates prepared from contralateral (intact) or distal crushed sciatic nerves
865 of WT and iDKO adult mice 5 dpi. c-Jun, active pS63-c-Jun and p75 are strongly upregulated in
866 iDKO, as in WT. Oct6 is strongly upregulated in WT and remains elevated before and after crush
867 in iDKO. (B) Quantification of Western blots. ns = not significant, 2-way ANOVA. c-Jun: WT
868 intact vs WT crushed, **P = 0.0035; WT intact vs iDKO intact, P = 0.9388; WT crushed vs
869 iDKO, P > 0.9999; iDKO intact vs iDKO crushed, **P = 0.0045. pc-Jun: WT intact vs WT
870 crushed, ***P = 0.0009; WT intact vs iDKO intact, P = 0.6737; WT crushed vs iDKO crushed, P
871 = 0.9962; iDKO intact vs iDKO crushed, **P = 0.0015. p75: WT intact vs WT crushed, *P =
872 0.0112; WT intact vs iDKO intact, P = 0.9993; WT crushed vs iDKO crushed, P = 0.5521; iDKO
873 intact vs iDKO crushed, **P = 0.0056. Oct6: WT intact vs WT crushed, *P = 0.0139; WT intact

874 vs iDKO intact, *P = 0.0157; WT crushed vs iDKO crushed, P = 0.2109; iDKO intact vs iDKO
875 crushed, P = 0.2541.

876

877 **Figure 4-figure supplement 1- source data 1**

878 **Source files for graphs quantifying c-Jun, pc-Jun, p75 and Oct6 Westerns.**

879 This zip archive contains the raw data for WT and iDKO used for the quantitative analysis
880 shown in Figure 4-S1. Data are in GraphPad Prism files, as indicated.

881

882 **Figure 5. Schwann cells lacking YAP/TAZ support axon regeneration**

883 (A) Schematic showing relative locations and sizes of the distal nerve segments used for
884 ultrastructural or light microscopic analysis of axon regeneration in WT or Yap/Taz iDKO, 12-
885 13 days after nerve crush. (B) Low magnification views of longitudinal sections of ~5 mm long
886 nerve segments distal to the crush site, showing regenerated axons in iDKO as abundant as in
887 WT. Axons are marked by TuJ1. (C, D) High magnification views of boxed area in (B), ~8 mm
888 distal to the crush site. (E) Low and high magnification views of TEM, taken at 5mm distal to the
889 crush site, showing numerous axons that regenerated within basal lamina tubes in iDKO, as in
890 WT. 'ax' denotes an axon. Numerous axons are large (>1µm) but unmyelinated in iDKO.
891 Examples of single large myelinated axons in WT (E-a, E-b), single large unmyelinated axon in
892 iDKO (E-c) and axon bundles containing a large unmyelinated axon in iDKO (E-d). (F)
893 Quantification of the axon density in crushed nerves of WT and iDKO, n = 4 mice for WT and 3
894 mice for iDKO. ns, not significant, P = 0.4715, Mann-Whitney. (G) Quantification of the
895 percentage of BL tubes containing axons in crushed nerves of WT and iDKO, n = 4 mice for WT
896 and 3 mice for iDKO. ns, not significant, P = 0.7237, Mann-Whitney (H) Quantification of the
897 percentage of BL tubes containing at least one axon > 1µm in diameter, in crushed nerves of WT
898 and iDKO. n = 4 mice for WT and 3 mice for iDKO. ns, not significant, P = 0.1573, Mann-
899 Whitney. (I) Quantification of the percentage of BL tubes containing multiple axons, at least one
900 of which is > 1µm in diameter, in crushed nerves of WT and iDKO. n = 4 mice for WT and 3
901 mice for iDKO. *P = 0.0339, Mann-Whitney. Scale bars = 500µm (B), 100µm (C, D), 2µm (E).

902

903 **Figure 5-source data 1**

904 **Source files for TEM data**

905 This zip archive contains the TEM images for one WT and one iDKO used for quantitative
906 analysis shown in Figures 5 G-I. Images were taken using a JEOL 1010 electron microscope
907 fitted with a Hamamatsu digital camera and AMT Advantage image capture software. Contrast
908 of the images was adjusted using Photoshop software. The images in this archive were also used
909 for the analysis in Figure 7.

910

911 **Figure 5- source data 2**

912 **Source files for graphs quantifying TEM data**

913 This zip archive contains the raw data for WT and iDKO used for the quantitative analysis
914 shown in Figures 5F, 5G, 5H and 5I. The data is contained in both a text document and an Excel
915 file, both labeled as Mann Whitney data. These files also contain data for Figures 3, 3-S1, 4, 6, 7,
916 8A and 8-S1E.

917

918 **Figure 6. Schwann cells lacking YAP/TAZ support timely axon regeneration after acute** 919 **injury**

920 (A) Schematic showing relative locations of crushed site, axon quantification and sizes of the
921 distal nerve segments used for light microscopic analysis of axon regeneration in WT or Yap/Taz
922 iDKO, 3 days after nerve crush. (B) Low magnification views of longitudinal sections, showing
923 abundant axon regeneration in both WT and iDKO. Regenerating axons are marked by SCG10.
924 (C, D) High magnification views of boxed areas in (B), showing numerous thin regenerating
925 axons. (E) Quantification of the axon density measured at 2 mm distal to the crushed site. $n = 3$
926 mice per genotype. ns, not significant, $P = 0.2752$, Mann-Whitney. (F) Quantification of the
927 distance regenerated by the longest axon. $n = 3$ mice per genotype. ns, not significant, $P = 0.8273$,
928 Mann-Whitney. Scale bars = 1mm (B), 100 μ m (C, D).

929

930 **Figure 6- source data 1**

931 **Source files for graphs quantifying axon density and length of longest axon**

932 This zip archive contains the raw data for WT and iDKO used for the quantitative analysis
933 shown in Figures 6E and 6F. The data is contained in both a text document and an Excel file,
934 both labeled as Mann Whitney data. These files also contain data for Figures 3, 3-S1, 4, 5, 7, 8A
935 and 8-S1E.

936

937 **Figure 7. Schwann cells lacking YAP/TAZ fail to myelinate regenerated axons**

938 Ultrastructural and light microscopic analyses of remyelination in distal nerves of WT or
939 Yap/Taz iDKO, 12-13 days after nerve crush. (A) Low magnification views of longitudinal
940 sections of intact or crushed nerves of WT and iDKO, showing no myelination of regenerated
941 axons in crushed nerves of iDKO as indicated by the lack of MBP immunostaining. Refer to
942 Figure 5B for robustly regenerated axons in the same iDKO mouse. (B, C) High magnification
943 views of boxed area in (A), showing abundant regenerated axons in crushed nerves of both WT
944 (B) and iDKO (C). Note that regenerated axons in iDKO are not myelinated. Axons and myelin
945 are marked by TuJ1 and MBP, respectively. (D) Semi-thin sections stained with toluidine blue
946 showing numerous myelinated axons in crushed nerves of WT but not in iDKO. (E) TEM images
947 of representative single large axons, myelinated in WT (left panel) but unmyelinated in iDKO
948 (right panel). (F) Quantification of the percentage of single axons that are myelinated. $n = 4$ mice
949 for WT and 3 mice for iDKO. $*P = 0.0323$, Mann-Whitney. (G) G-ratio in WT and iDKO.
950 Myelinated axons in WT are compared to unmyelinated single axons in iDKO. $n = 3$ mice per
951 genotype. $*P = 0.0495$ Mann-Whitney. Scale bars = $500\mu\text{m}$ (A), $100\mu\text{m}$ (B, C), $10\mu\text{m}$ (D), $2\mu\text{m}$
952 (E).

953

954 **Figure 7-source data 1**

955 **Source files for TEM data**

956 This zip archive contains the TEM images for one WT and one iDKO used for quantitative
957 analysis shown in Figures 7 F and 7 G. Images were taken using a JEOL 1010 electron
958 microscope fitted with a Hamamatsu digital camera and AMT Advantage image capture software.
959 Contrast of the images was adjusted using Photoshop software. The images in this archive were
960 also used for the analysis in Figure 5.

961

962 **Figure 7- source data 2**

963 **Source files for graphs quantifying TEM data**

964 This zip archive contains the raw data for WT and iDKO used for the quantitative analysis
965 shown in Figures 7F and 7G. The data is contained in both a text document and an Excel file,

966 both labeled as Mann Whitney data. These files also contain data for Figures 3, 3-S1, 4, 5, 6, 8A
967 and 8-S1E.

968

969 The following figure supplements are available for Figure 7.

970 **Figure 7-figure supplement 1**

971 **Additional images of axon regeneration and remyelination in WT and *Yap/Taz* iDKO**

972 High magnification views of longitudinal sections of intact or crushed nerves of WT and iDKO,
973 12-13 days after nerve crush. Axons and myelin are marked by TuJ1 (green) and MBP (red),
974 respectively. Numerous axons regenerated in crushed nerves of iDKO, as in WT, but they are
975 unmyelinated. Myelin remains ample, as indicated by abundant MBP, in contralateral intact
976 nerves of iDKO at 12-13 dpi. Scale bar = 50 μ m.

977

978 **Figure 8. YAP and TAZ are redundantly required for optimal remyelination**

979 (A) Western blotting of intact sciatic nerve lysates, showing markedly reduced TAZ in *Taz* iKO,
980 whereas YAP levels remain relatively unchanged. YAP band is tighter and faster migrating in
981 *Taz* iKO, than in WT, indicative of reduced phosphorylation. Quantification of Yap and Taz in
982 WT and *Taz* iKO, n = 3 mice per genotype. YAP: ns, not significant, P = 0.2752, Mann-Whitney.
983 TAZ: *P = 0.0495, Mann-Whitney. (B) Quantification of axon density in WT, *Yap/Taz* iDKO
984 and *Taz* iKO nerves at 12 dpi, 8-10 mm distal to crush site (also see Figures 5B, F and Figure 8-
985 figure supplement 1B, E). n = 4 mice for WT, 3 mice for iDKO and *Taz* iKO: WT vs iDKO, P =
986 0.72; WT vs iKO, P = 0.41; iDKO vs iKO, P = 0.18, all not significant, one-way ANOVA with
987 Tukey's multiple comparison test. (C-G) Comparative analysis of axon regeneration and
988 remyelination in WT and *Taz* iKO, 12-13 days after nerve crush. (C) Representative TEM
989 images of WT and *Taz* iKO nerves, taken at 5mm distal to the crush site, showing numerous
990 axons that regenerated within basal lamina tubes in *Taz* iKO, as in WT. 'ax' denotes a single
991 axon. Some large axons are myelinated in *Taz* iKO. (D) Quantification of the percentage of BL
992 tubes containing axons of any diameter in WT, *Taz* iKO and *Yap/Taz* iDKO nerves. n = 4 mice
993 for WT, 3 mice for iDKO and 2 mice for *Taz* iKO : WT vs. iDKO, P = 0.99; WT vs. iKO, P
994 =0.90; iDKO vs. *Taz* iKO, P = 0.92, all not significant, one-way ANOVA with Tukey's multiple
995 comparison test. (E) Quantification of the percentage of BL tubes containing at least 1 axon
996 larger than 1 μ m in diameter in WT, *Taz* iKO and *Yap/Taz* iDKO nerves. n = 4 mice for WT, 3

997 mice for iDKO and 2 mice for *Taz* iKO: WT vs. iDKO, $P = 0.73$; WT vs. iKO, $P = 0.22$; iDKO
998 vs. iKO, $P = 0.52$, all not significant, one-way ANOVA with Tukey's multiple comparison test.
999 (F) Quantification of the percentage of single axons that are remyelinated in WT, *Taz* iKO and
1000 *Yap/Taz* iDKO nerves. $n = 4$ mice for WT, 3 mice for iDKO and 2 mice for *Taz* iKO: WT vs.
1001 iDKO, **** $P < 0.0001$; WT vs. iKO, ** $P = 0.0094$; iDKO vs. *Taz* iKO, ** $P = 0.0016$, one-way
1002 ANOVA with Tukey's multiple comparison test. (G) G-ratios of remyelinated axons in WT and
1003 *Taz* iKO nerves, compared to unmyelinated axons in *Yap/Taz* iDKO nerve. WT and *Taz* iKO
1004 remyelinated axons have equivalent G-ratios. $n = 6$ mice for WT, 3 mice for iDKO and 2 mice
1005 for iKO: WT vs. iDKO, **** $P < 0.0001$; WT vs. iKO, not significant, $P = 0.074$; iDKO vs. iKO,
1006 *** $P = 0.0008$, one-way ANOVA with Tukey's multiple comparison test. Scale bar = $2\mu\text{m}$ (C).

1007

1008 **Figure 8-source data 1**

1009 **Source files for TEM data**

1010 This zip archive contains the TEM images for one WT and one *Taz* iKO used for quantitative
1011 analysis shown in Figures 8 D-G. Images were taken using a JEOL 1010 electron microscope
1012 fitted with a Hamamatsu digital camera and AMT Advantage image capture software. Contrast
1013 of the images was adjusted using Photoshop software.

1014

1015 **Figure 8- source data 2**

1016 **Source files for graphs quantifying Yap and Taz levels.**

1017 This zip archive contains the raw data for WT and iDKO used for the quantitative analysis
1018 shown in Figure 8A. The data is contained in both a text document and an Excel file, both
1019 labeled as Mann Whitney data. These files also contain data for Figures 3, 3-S1, 4, 5, 6, 7 and 8-
1020 S1E.

1021

1022 **Figure 8- source data 3**

1023 **Source files for graphs quantifying axon density and TEM data**

1024 This zip archive contains the raw data for WT, iDKO and *Taz* iKO used for the quantitative
1025 analysis shown in Figures 8B, 8D, 8E, 8F and 8G. The data is contained in GraphPad Prism files,
1026 as indicated.

1027 **Figure 8-source data 4.**

1028 **Loss of TAZ protein expression in sciatic nerves of *Taz* iKO mice**

1029 Uncropped Western blots of images used to make Figure 8A. Individually processed samples
1030 from 3 WT mice (#208,#211,#213) and 3 *Taz* iKO mice (#210,#216,#249) are shown and used
1031 for quantification. X.....X denotes the line along which membranes were cut prior to probing
1032 with the relevant antibodies .

1033

1034 The following figure supplements are available for Figure 8.

1035 **Figure 8-figure supplement 1**

1036 **Schwann cells expressing YAP (but lacking TAZ) support axon regeneration**

1037 A) Schematic showing relative locations and sizes of the distal nerve segments used for light
1038 microscopic and TEM analysis of axon regeneration in WT or *Taz* iDKO, 12 days after nerve
1039 crush. (B) Low magnification views of longitudinal nerve sections beginning 5 mm distal to the
1040 crush site, showing regenerated axons in iKO as abundant as in WT. Axons are marked by TuJ1.
1041 (C, D) High magnification views of boxed areas in (B). Scale bars = 1 mm (B) and 100 μ m (C,
1042 D). (E) Quantification of axon density measured at ~10 mm distal to the crush site. n = 3 mice
1043 per genotype. ns, not significant, P = 0.2118, Mann-Whitney.

1044

1045 **Figure 8-figure supplement 1- source data 1**

1046 **Source files for graph quantifying axon density.**

1047 This zip archive contains the raw data for WT and *Taz* iKO used for the quantitative analysis
1048 shown in Figure 8-S1E. The data is contained in both a text document and an Excel file, both
1049 labeled as Mann Whitney data. These files also contain data for Figures 3, 3-S1, 4, 5, 6, 7 and 8.

1050

1051 **Figure 9. Redifferentiation of Schwann cells lacking YAP/TAZ**

1052 Longitudinal sections of crushed nerves of WT and *Yap/Taz* iDKO at 12 dpi, immunostained by
1053 various markers of SC dedifferentiation (c-Jun and Oct-6), proliferation (Ki67) and
1054 redifferentiation (Krox20). SCs are marked by Sox10. (A) Representative sections showing c-
1055 Jun+ SCs markedly reduced in iDKO, as in WT. (B) Representative sections showing rarely
1056 observed Ki67+ proliferating SCs in iDKO, as in WT. (C) Representative sections showing Oct-
1057 6+ SCs reduced in iDKO, as in WT. (D) Representative sections showing failed upregulation of
1058 Krox20 in iDKO SCs. (E) Quantitative comparison of c-Jun+ SCs at 5 and 12 dpi, showing

1059 similar downregulation of c-Jun in WT and iDKO SC. n=3 mice per genotype, 2-way ANOVA,
1060 ns = not significant. WT 5 dpi vs WT 12 dpi, **P = 0.0069; WT 5 dpi vs iDKO 5 dpi, P =
1061 0.4260; WT 12 dpi vs iDKO 12 dpi, P = 0.9574; iDKO 5 dpi vs iDKO 12 dpi, **P = 0.0018. (F)
1062 Quantitative comparison of Ki67+ SCs, showing similar reduction in proliferating SCs in WT
1063 and iDKO nerves between 5 dpi and 12 dpi. n=3 mice per genotype, 2-way ANOVA, ns = not
1064 significant. WT 5 dpi vs WT 12 dpi, ****P < 0.0001; WT 5 dpi vs iDKO 5 dpi, P > 0.9999; WT
1065 12 dpi vs iDKO 12 dpi, P = 0.6775; iDKO 5 dpi vs iDKO 12 dpi, ****P < 0.0001. (G)
1066 Quantitative comparison of Oct-6+ SCs, showing significant downregulation of Oct-6 in WT and
1067 iDKO SCs between 5 dpi and 12 dpi. n=3 mice per genotype, ns = not significant, 2-way
1068 ANOVA. WT 5 dpi vs WT 12 dpi, ***P = 0.0005; WT 5 dpi vs iDKO 5 dpi, P = 0.9817; WT 12
1069 dpi vs iDKO 12 dpi, *P = 0.0221; iDKO 5 dpi vs iDKO 12 dpi, *P = 0.0299. (H) Quantitative
1070 comparison of Krox20+ SCs, showing upregulation of Krox20 in WT SCs, but not in iDKO SCs
1071 between 5 dpi and 12 dpi. n=3 mice per genotype, 2-way ANOVA, ns = not significant. WT 5
1072 dpi vs WT 12 dpi, ****P < 0.0001; WT 5 dpi vs iDKO 5 dpi, P > 0.9999; WT 12 dpi vs iDKO
1073 12 dpi, ****P < 0.0001; iDKO 5 dpi vs iDKO 12 dpi, P > 0.9999. Scale bar = 10µm (A-D).

1074

1075 **Figure 9-source data 1**

1076 **Source files for Krox20⁺ SC data**

1077 This zip archive contains the IHC for one WT and one iDKO used for quantitative analysis
1078 shown in Figure 9E. Leica SP8 confocal lif images were processed using Imaris software and
1079 saved as tiffs.

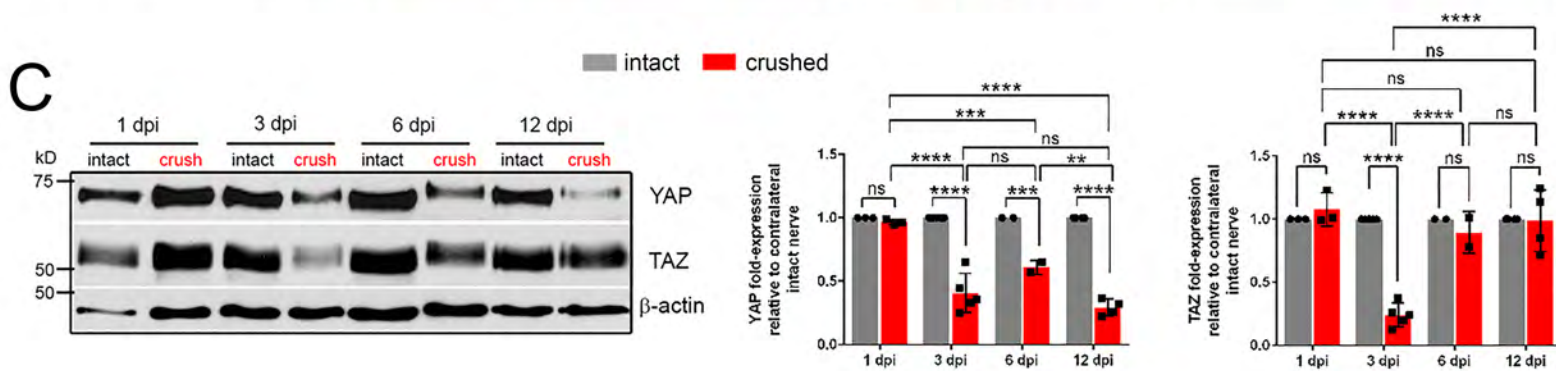
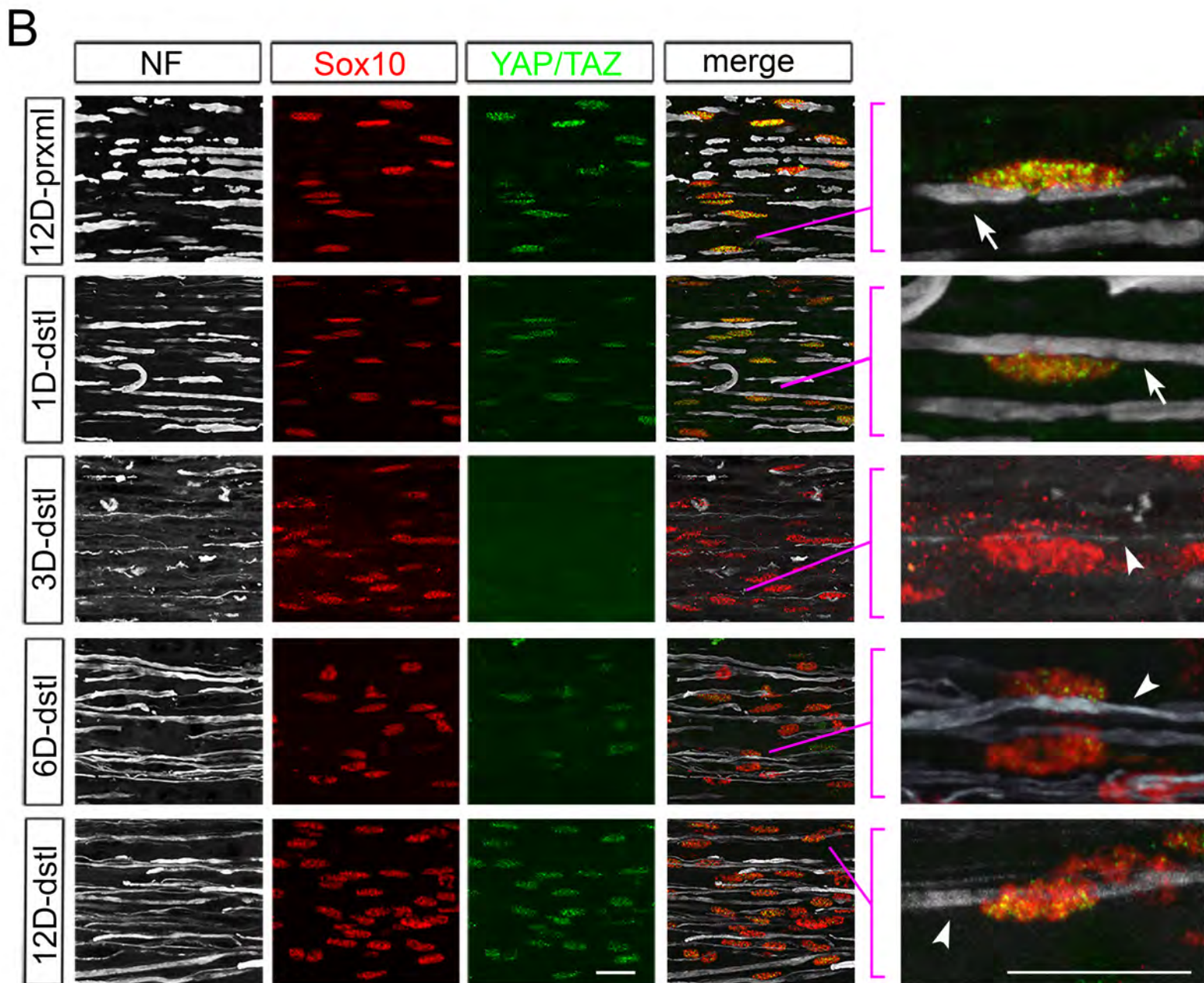
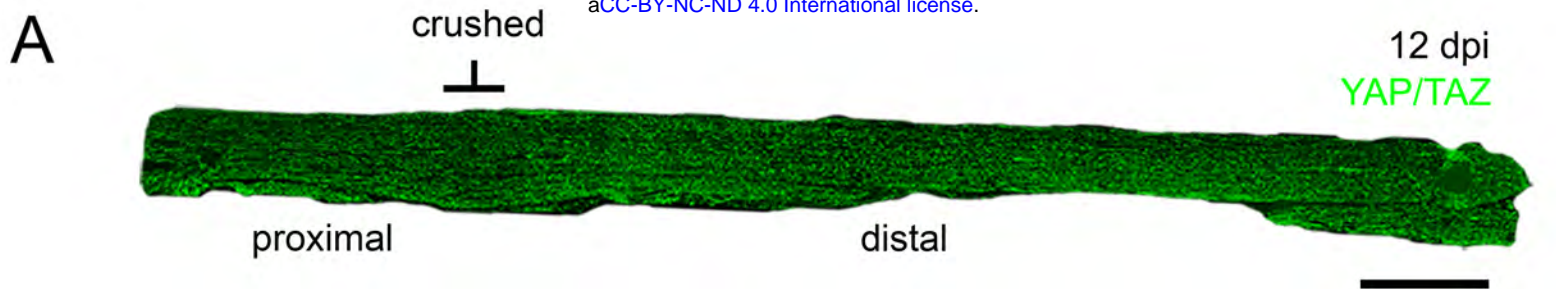
1080

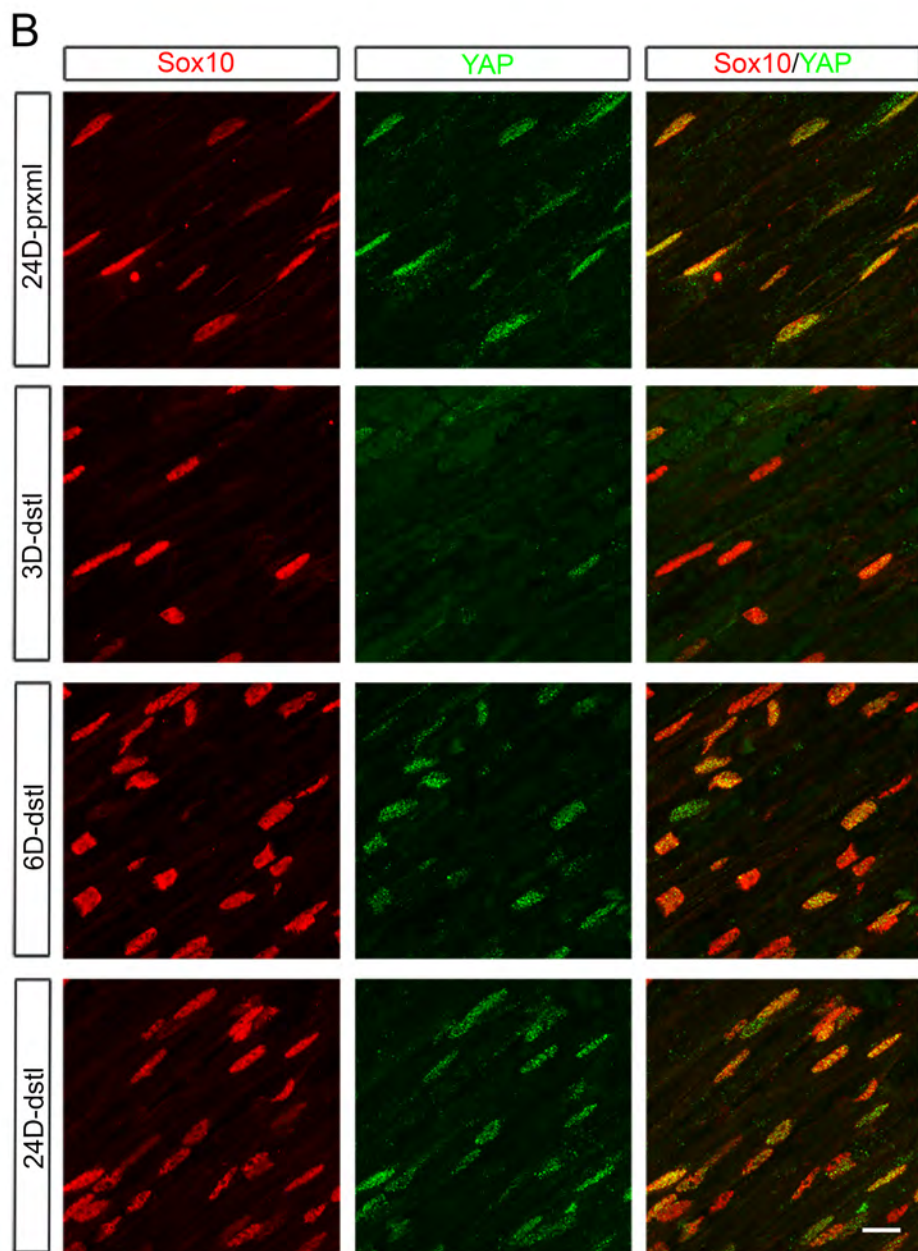
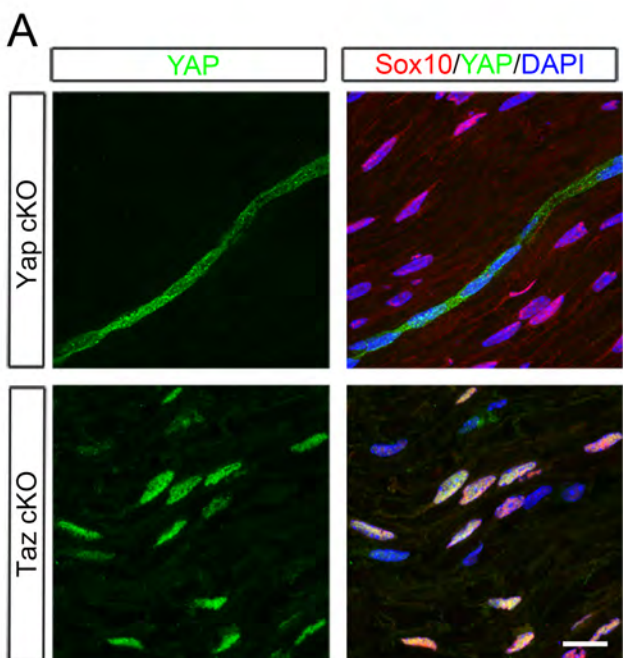
1081 **Figure 9- source data 2**

1082 **Source files for graphs quantifying c-Jun+ SCs, Ki67+ SCs, Oct6+ SCs and Krox20+ SCs**

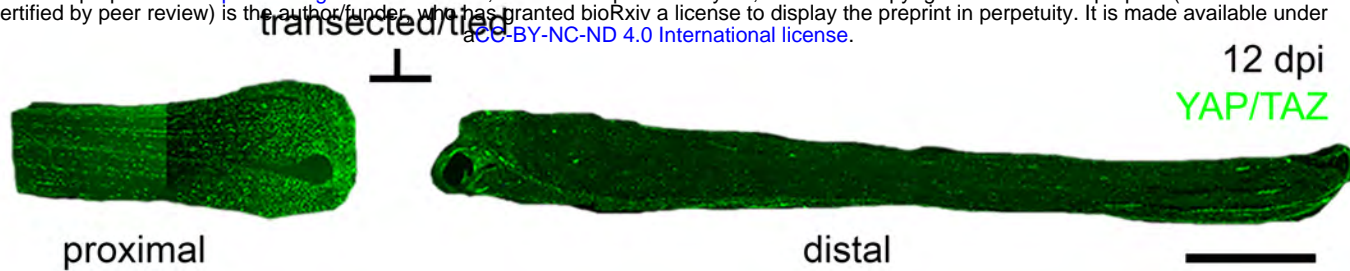
1083 This zip archive contains the raw data for WT and iDKO used for the quantitative analysis
1084 shown in Figures 9E, 9F, 9G and 9H. The data is contained in GraphPad Prism files, as indicated.

1085

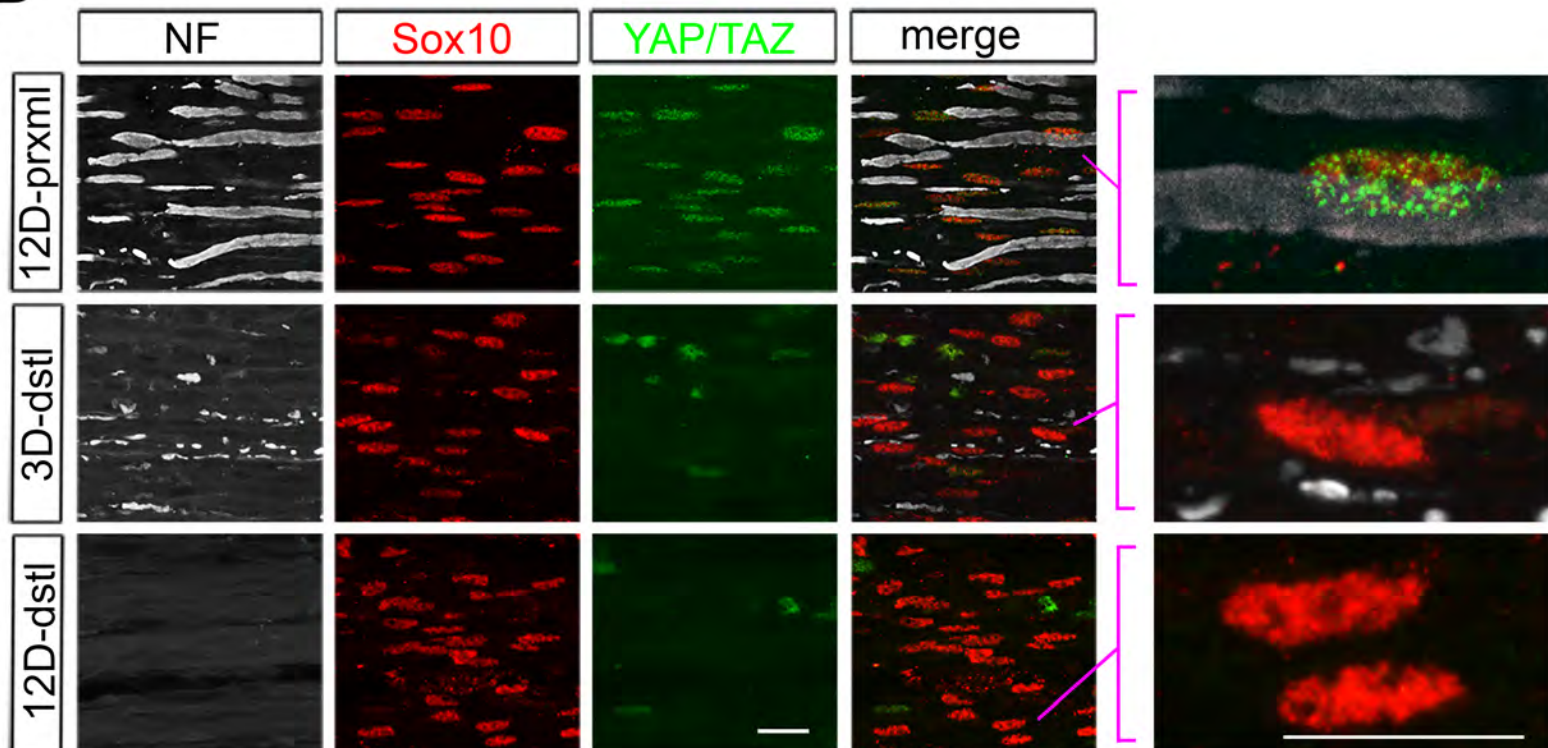




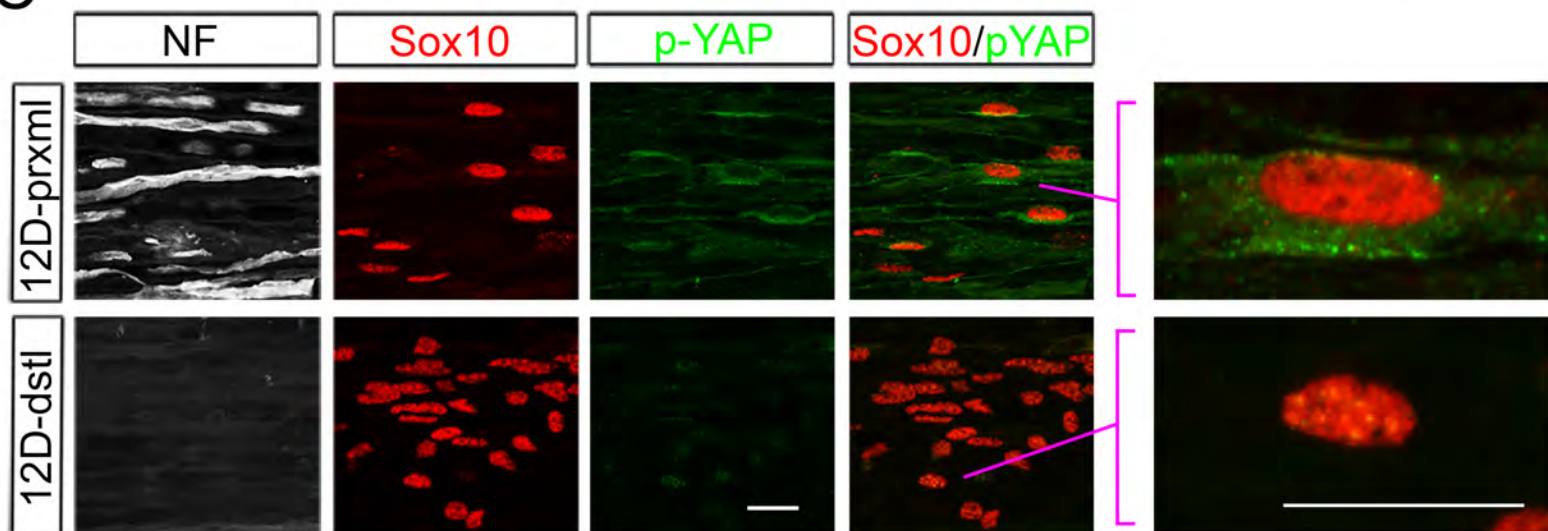
A



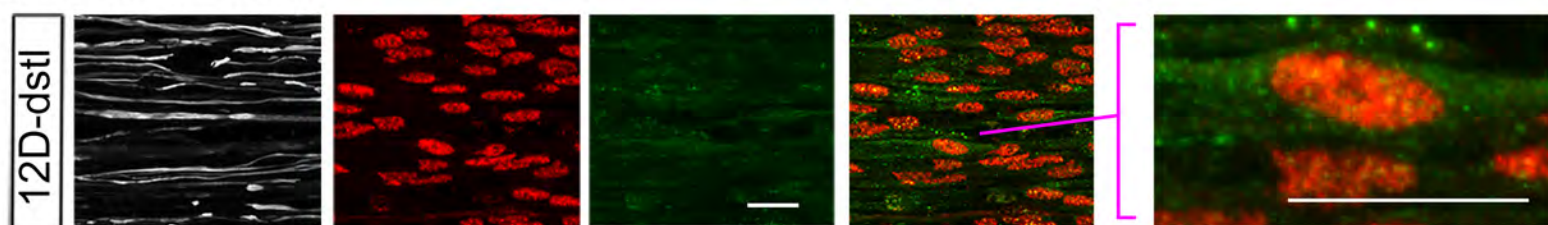
B

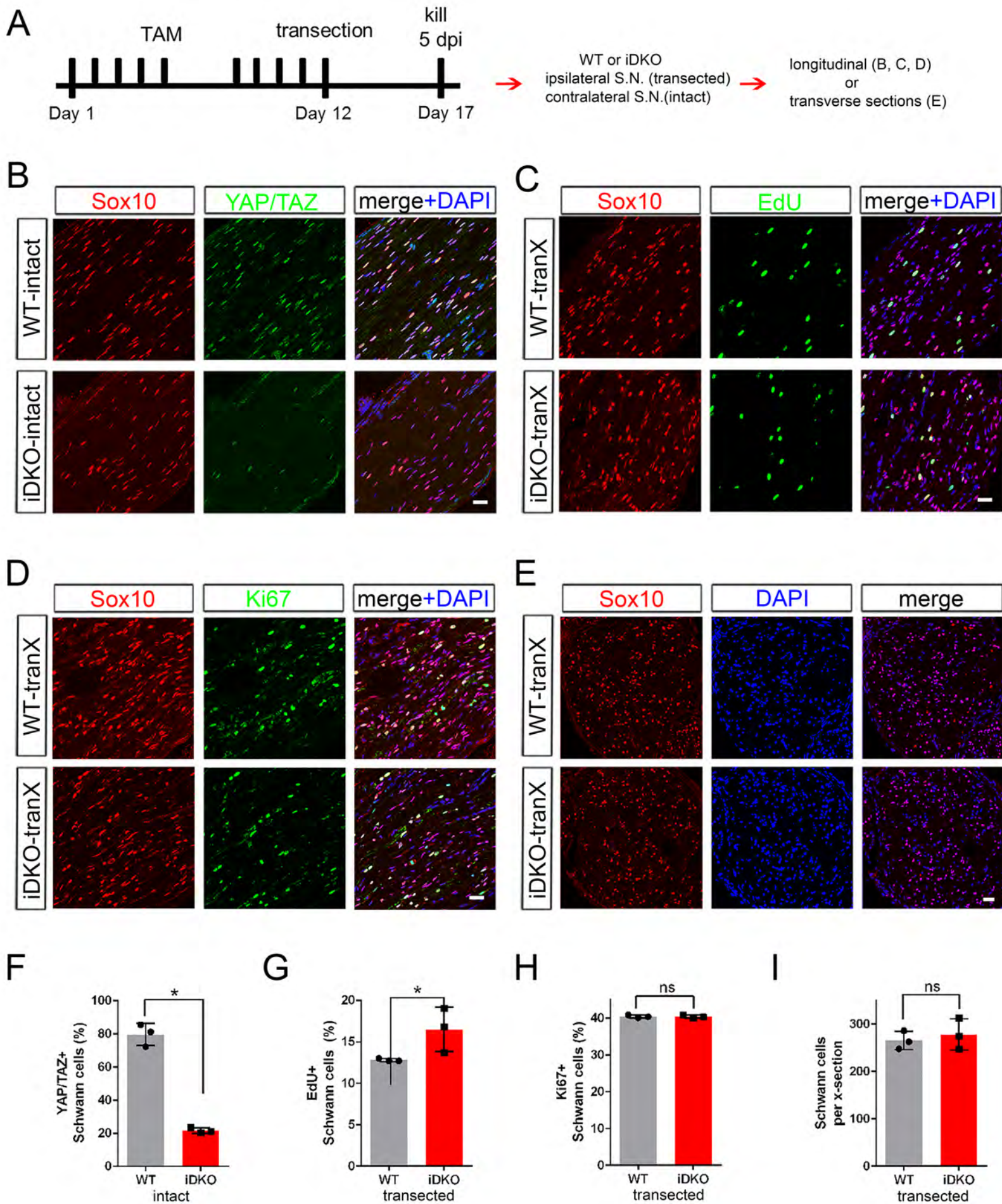


C

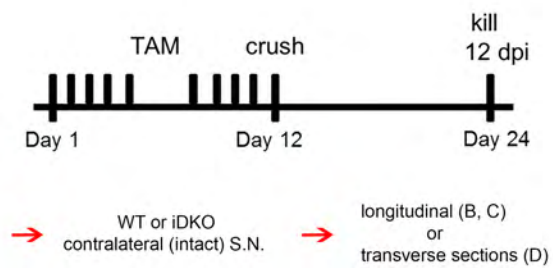


D crushed nerve

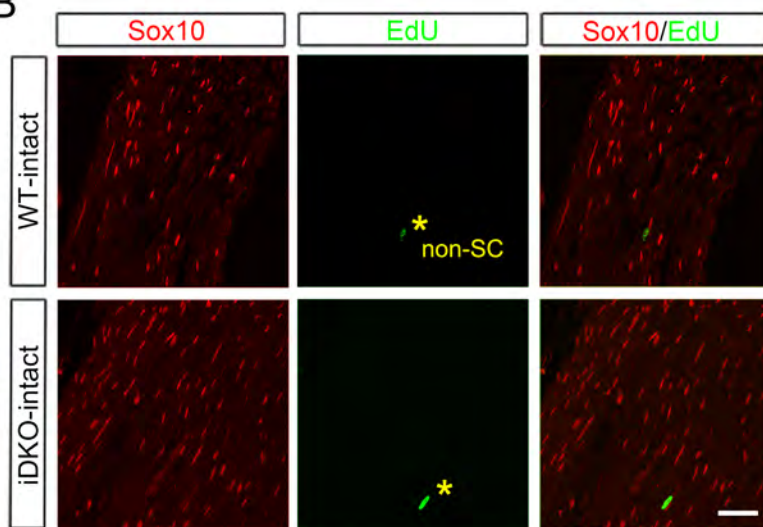




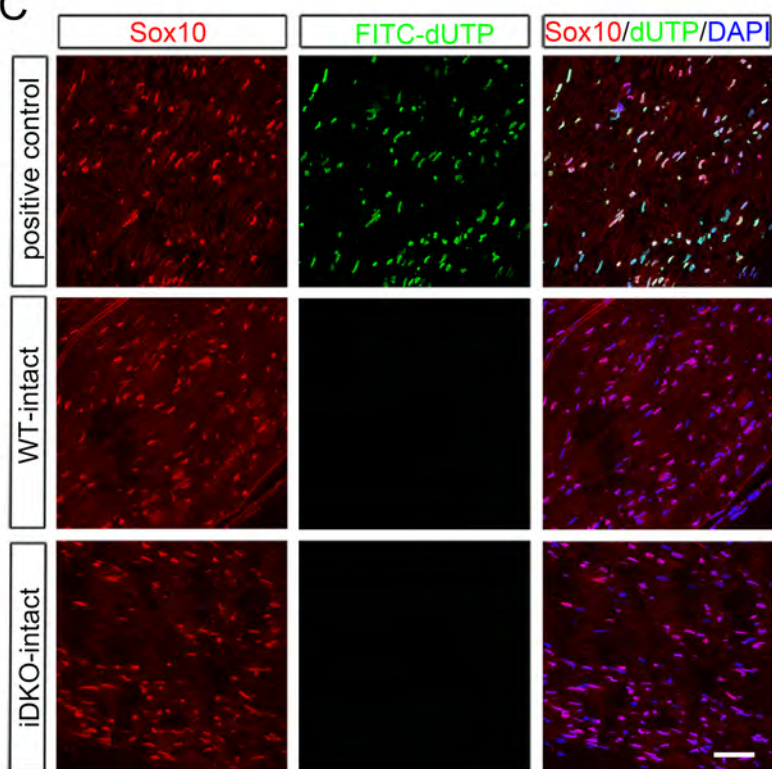
A



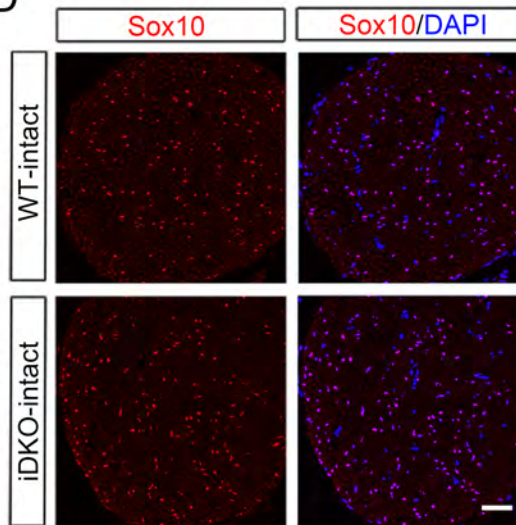
B



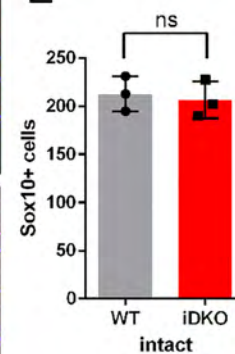
C

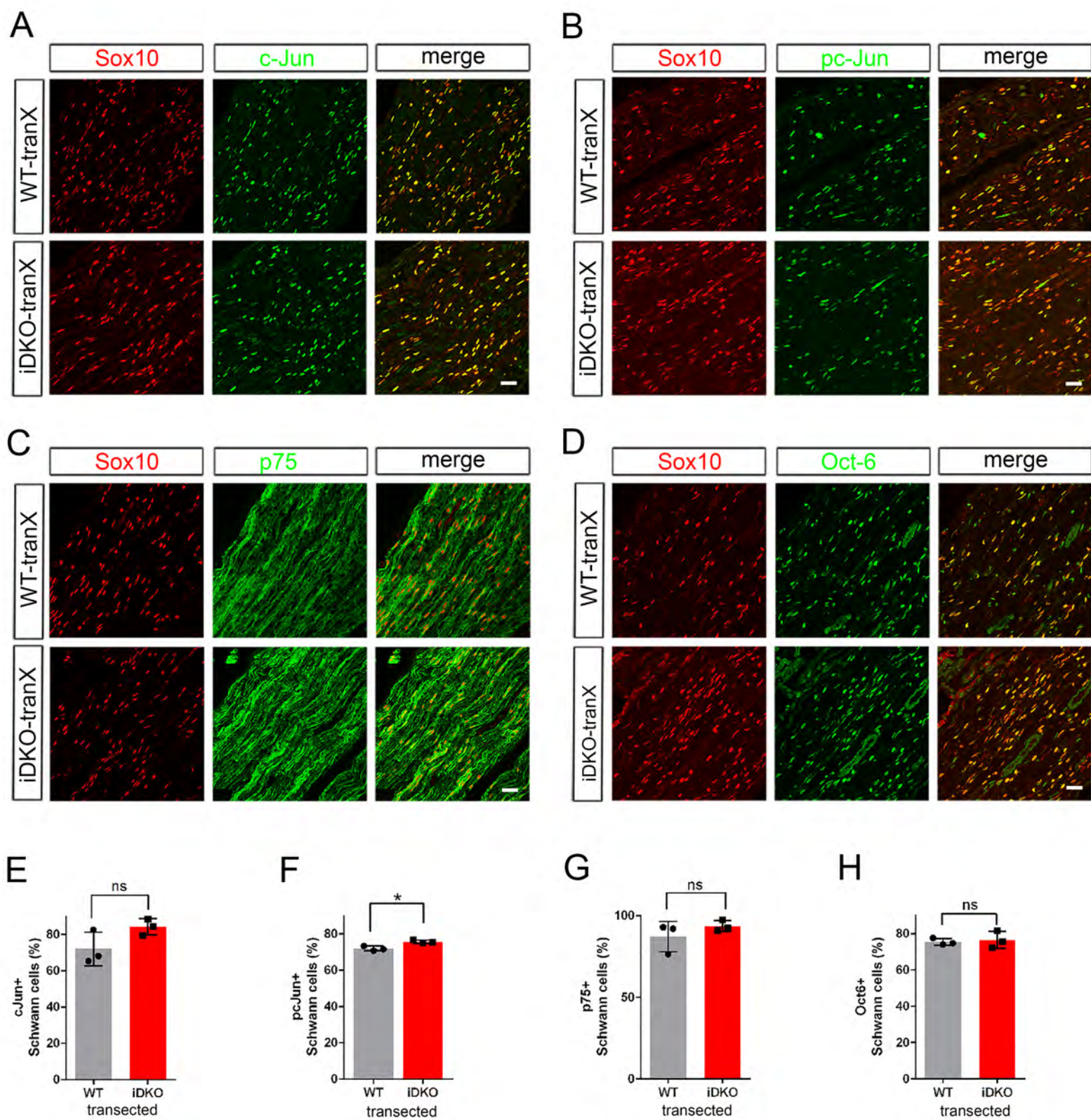


D

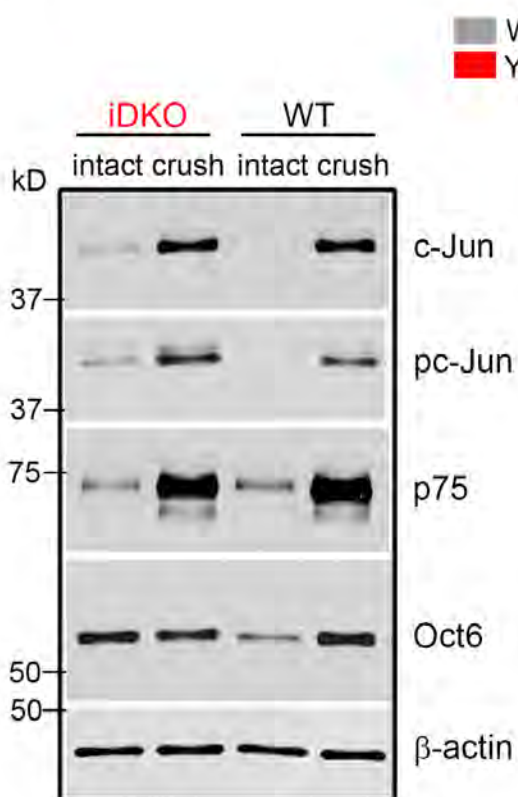


E

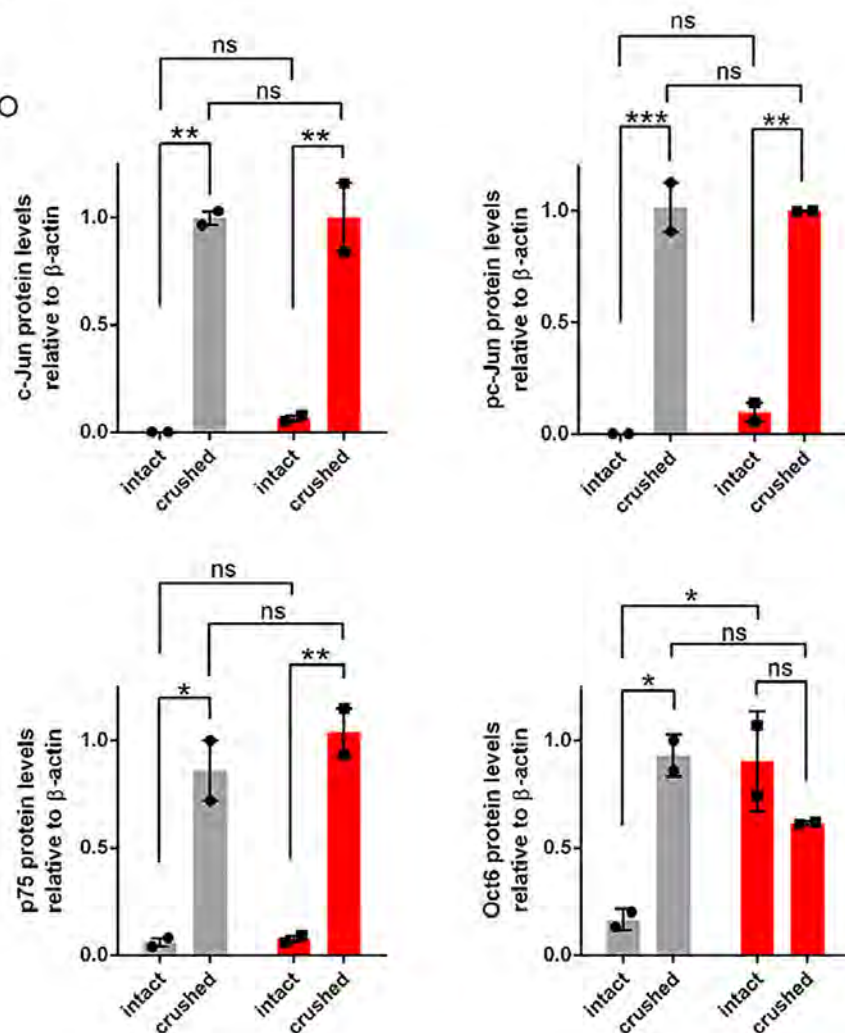


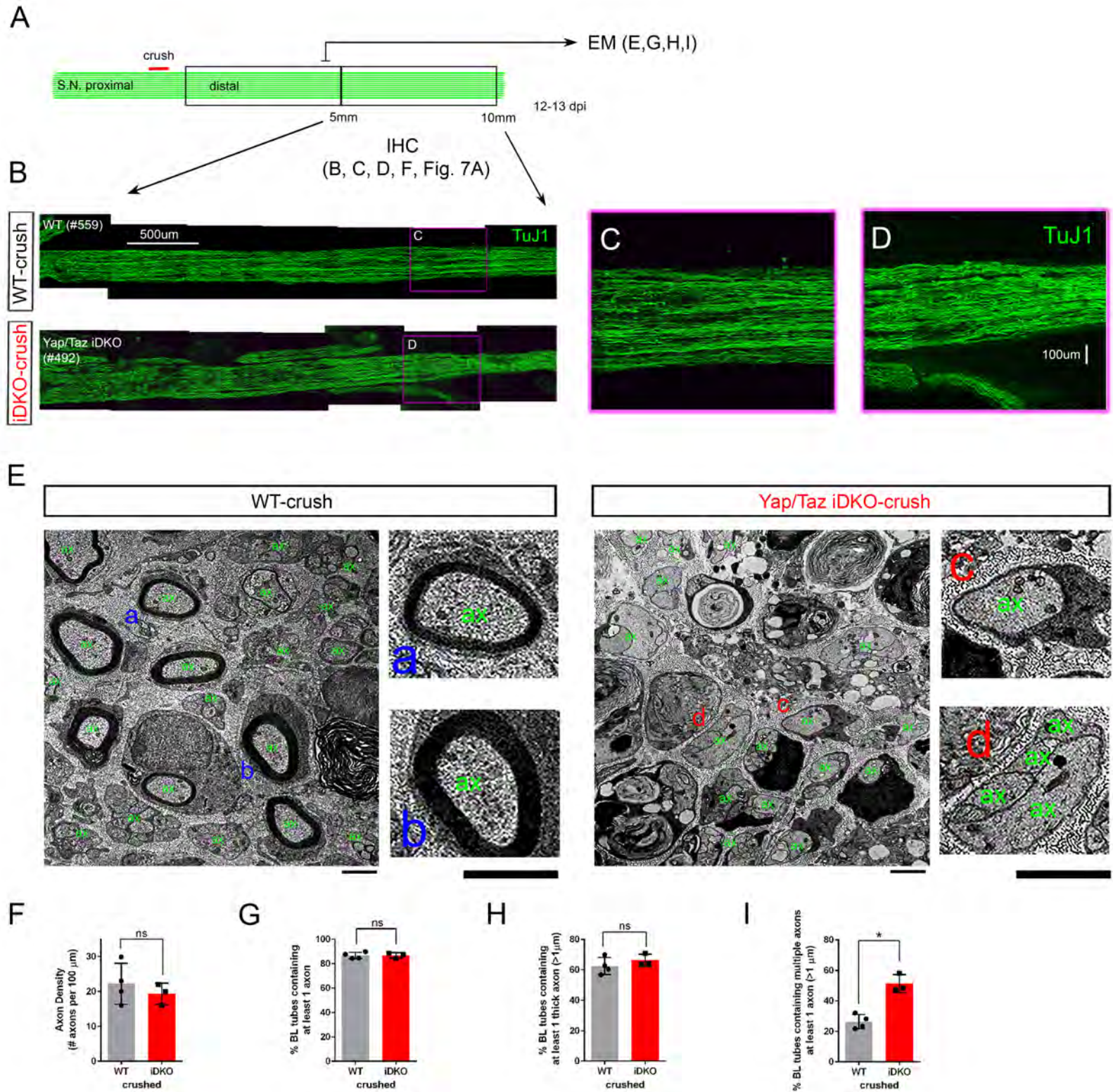


A

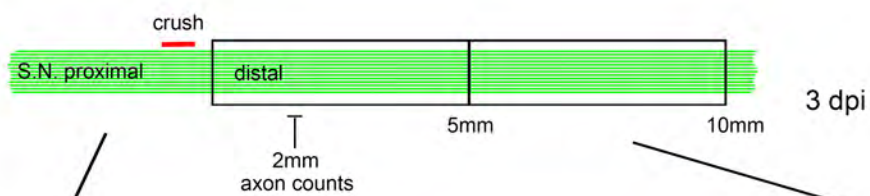


B

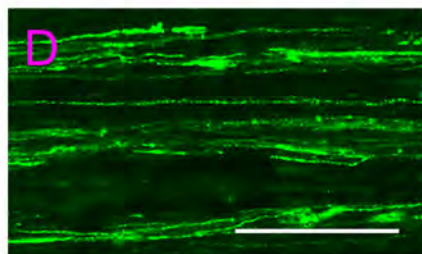
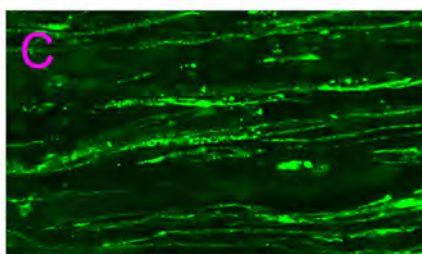
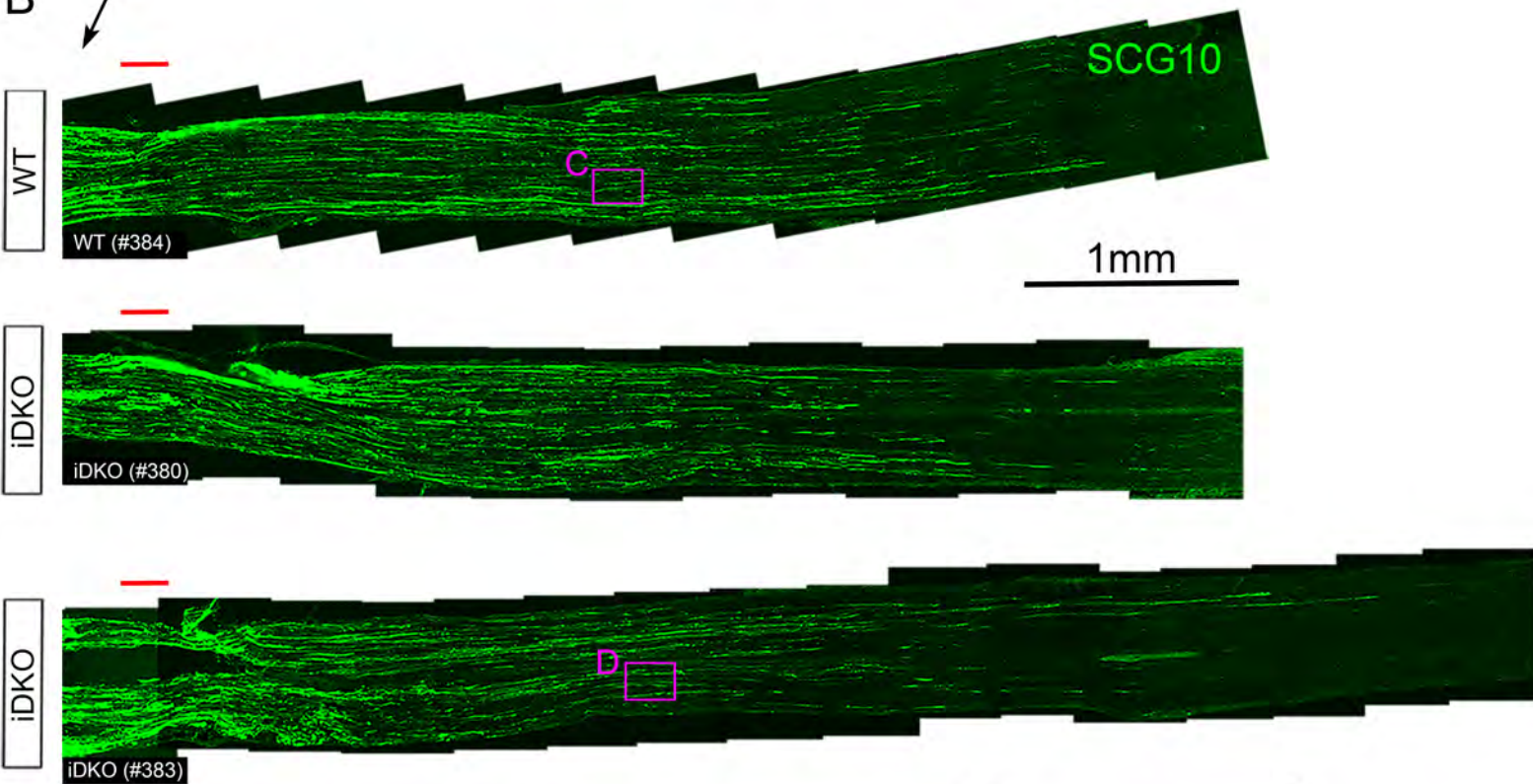




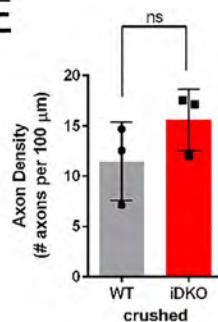
A



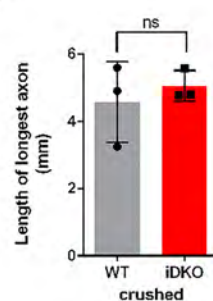
B

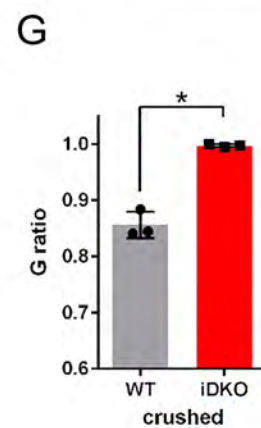
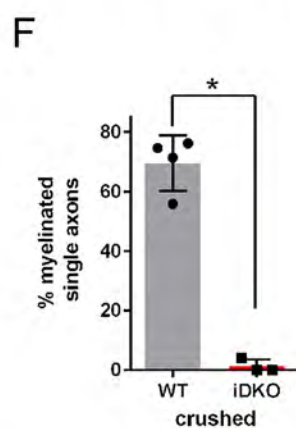
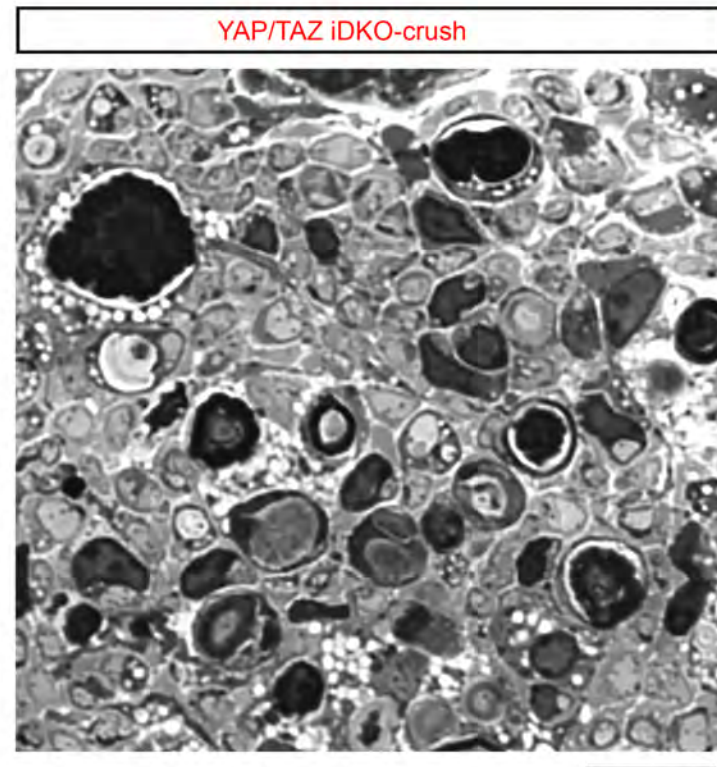
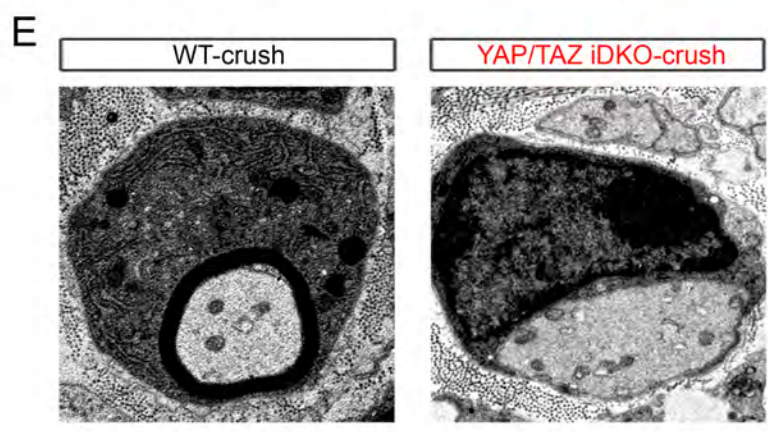
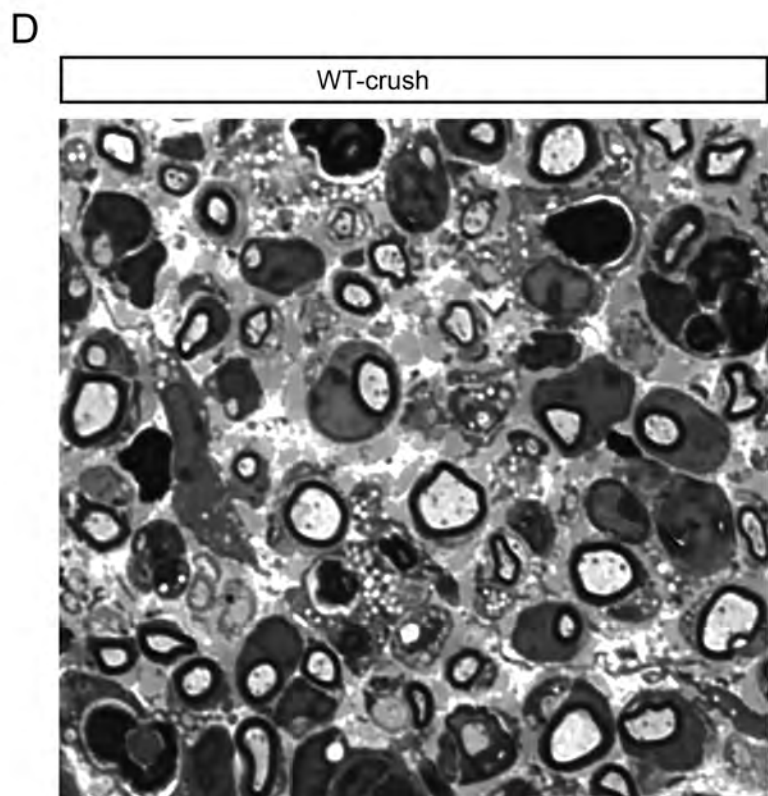
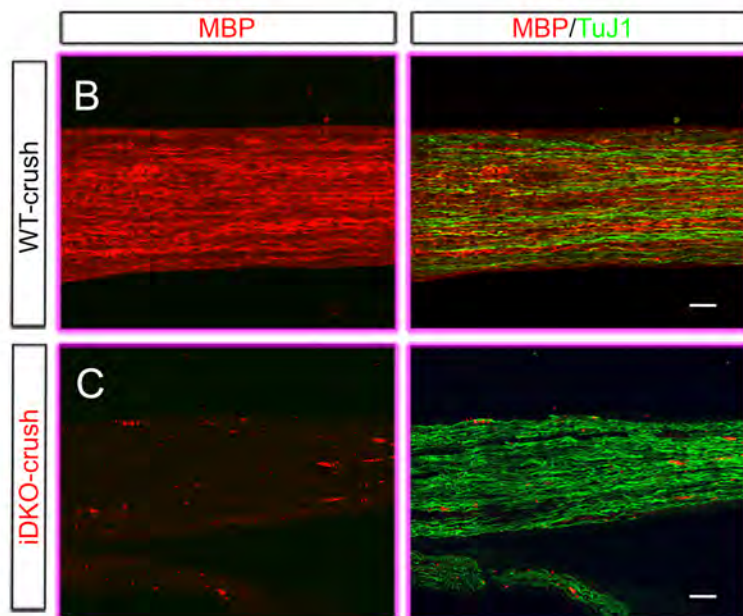
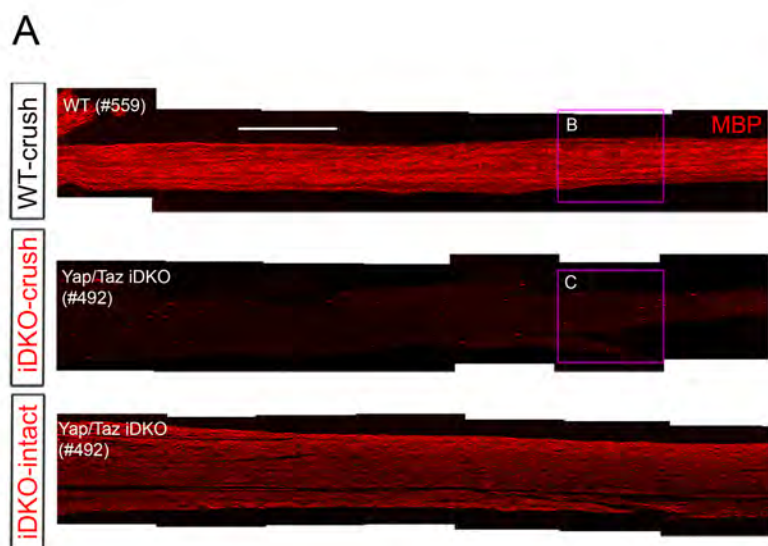


E



F



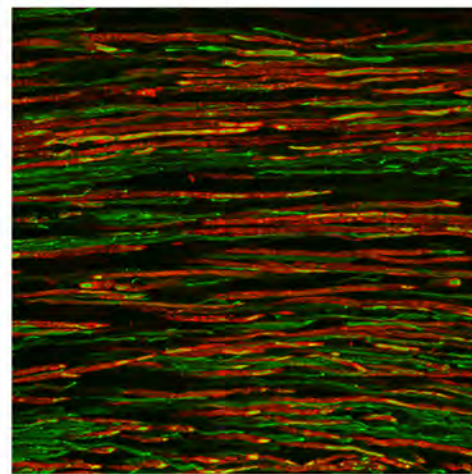
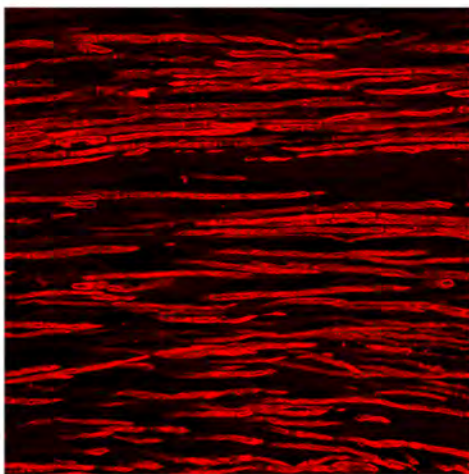
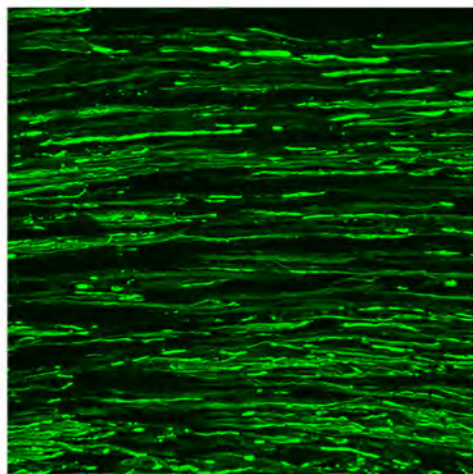


TUJ1

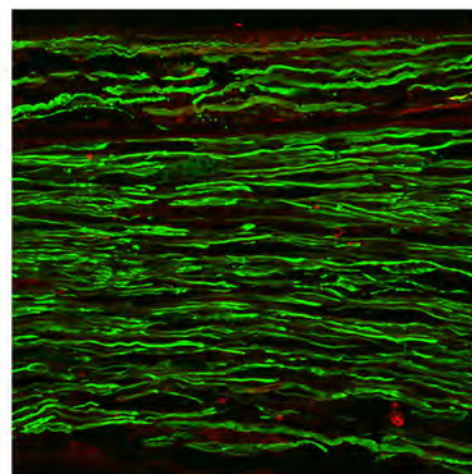
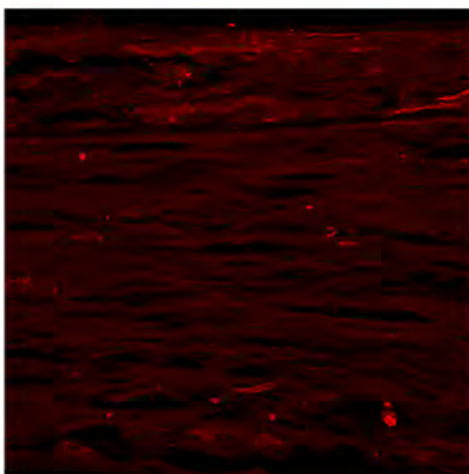
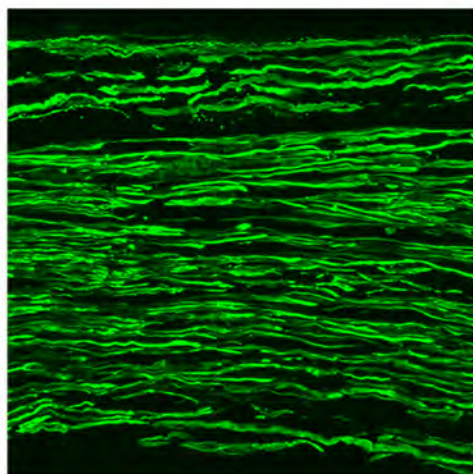
MBP

MBP/TUJ1

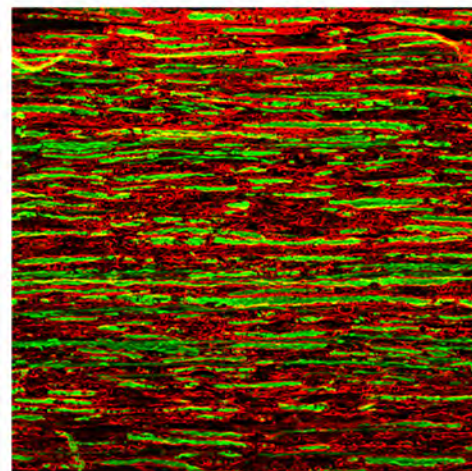
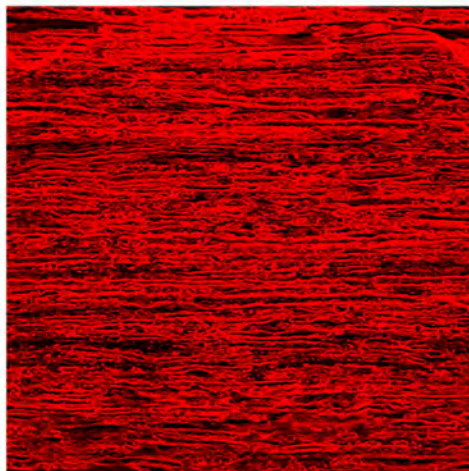
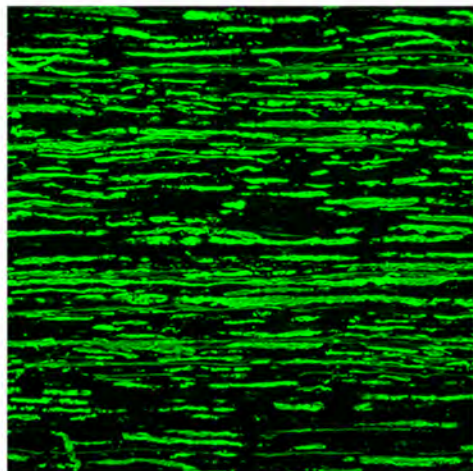
WT-crush



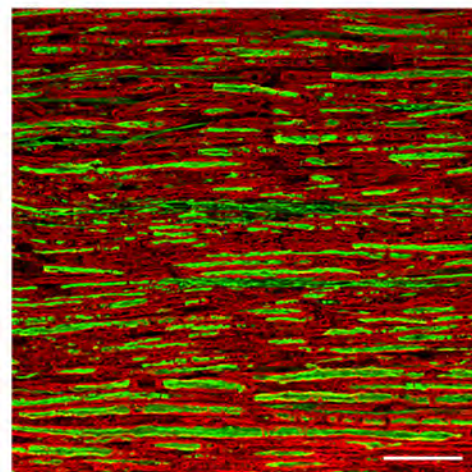
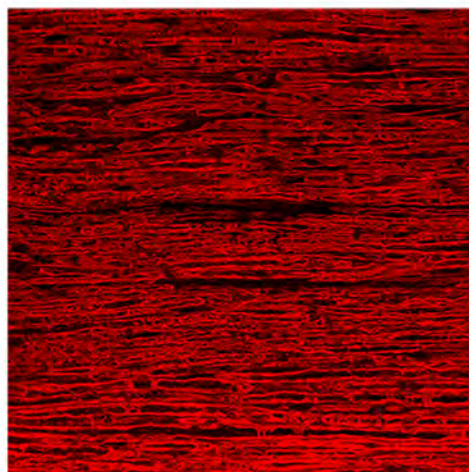
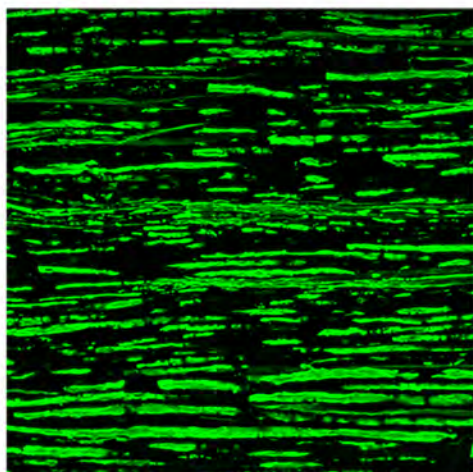
iDKO-crush



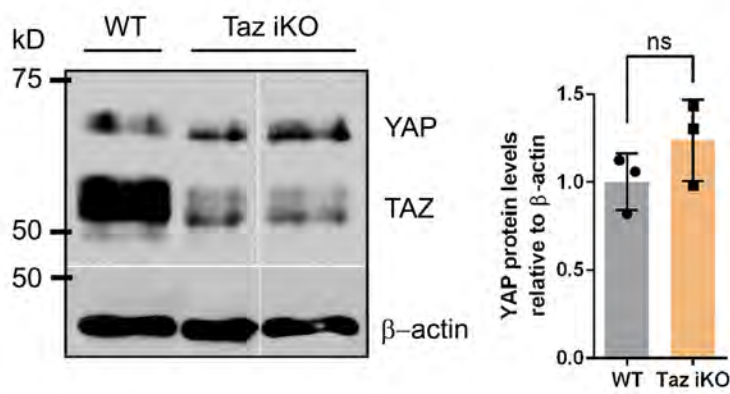
WT-intact



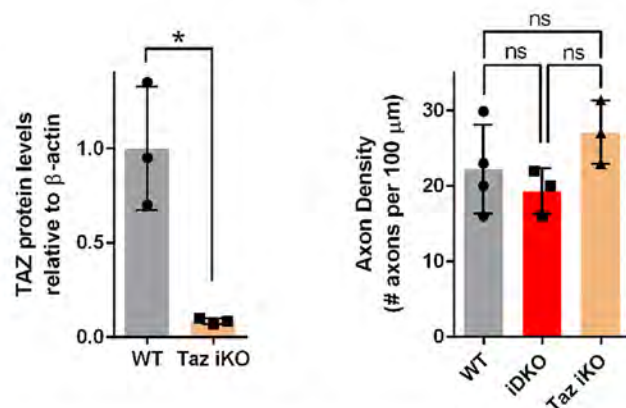
iDKO-intact



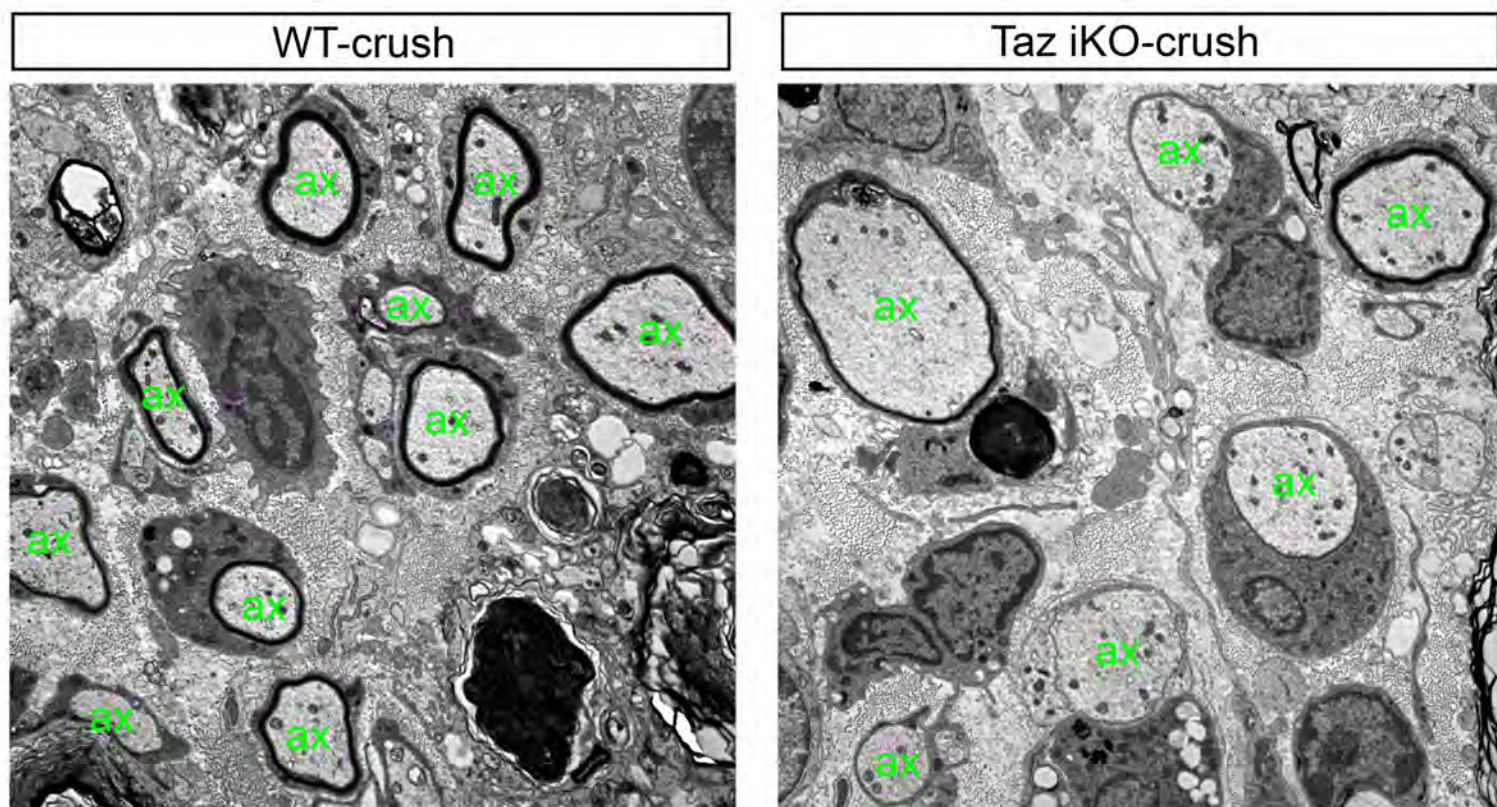
A



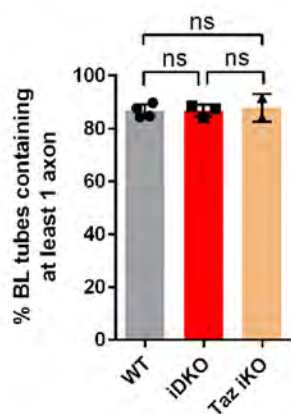
B



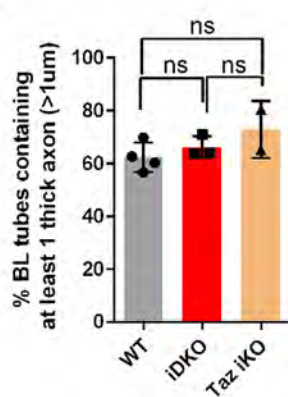
C



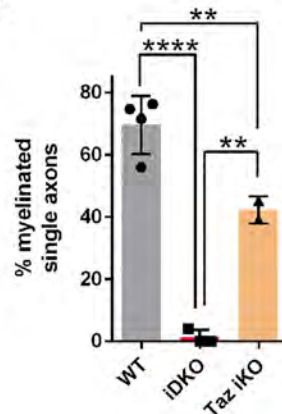
D



E



F



G

